

# Linking Early and Late Type Galaxies to their Dark Matter Haloes

Frank C. van den Bosch<sup>1</sup>, Xiaohu Yang<sup>1,2</sup>, and H.J. Mo<sup>1</sup> <sup>★</sup>

<sup>1</sup>Max-Planck-Institut für Astrophysik, Karl Schwarzschild Str. 1, Postfach 1317, 85741 Garching, Germany

<sup>2</sup>Center for Astrophysics, University of Science and Technology of China, Hefei 230026, China

Accepted ..... Received .....; in original form .....

## ABSTRACT

Using data from the 2 degree Field Galaxy Redshift Survey (2dFGRS) we compute the conditional luminosity functions (CLFs) of early- and late-type galaxies. These functions give the average number of galaxies with luminosities in the range  $L \pm dL/2$  that reside in a halo of mass  $M$ , and are a powerful statistical tool to link the distribution of galaxies to that of dark matter haloes. Although some amount of degeneracy remains, the CLFs are well constrained. They indicate that the average mass-to-light ratios of dark matter haloes have a minimum of  $\sim 100h$  (M/L)<sub>○</sub> around a halo mass of  $\sim 3 \times 10^{11}h^{-1}$  M<sub>○</sub>. Towards lower masses  $\langle M/L \rangle$  increases rapidly, and matching the faint-end slope of the observed luminosity function (LF) requires that haloes with  $M < 10^{10}h^{-1}$  M<sub>○</sub> are virtually devoid of galaxies. At the high mass end, the observed clustering properties of galaxies require that clusters have  $b_J$ -band mass-to-light ratios in the range  $500 - 1000h$  (M/L)<sub>○</sub>. Finally, the fact that early-type galaxies are more strongly clustered than late-type galaxies requires that the fraction of late-type galaxies is a strongly declining function of halo mass. We compute two-point correlation functions as function of both luminosity and galaxy type. The agreement with observations, in terms of normalization and power-law slope, is remarkably good. When including predictions for the correlation functions of faint galaxies we find a weak (strong) luminosity dependence for the late (early) type galaxies. We also investigate the inferred halo occupation numbers. Late-type and faint galaxies reveal a shallower  $\langle N \rangle(M)$  than bright, early-type galaxies, which explains why  $\langle N \rangle(M)$  transforms from a single power-law for bright galaxies to a more complicated form when fainter galaxies are included. Finally we compare our CLFs with predictions from several semi-analytical models for galaxy formation. As long as these models accurately fit the 2dFGRS luminosity function the agreement with our predictions is remarkably good. This indicates that the technique used here has recovered a statistical description of how galaxies populate dark matter haloes which is not only in perfect agreement with the data, but which in addition fits nicely within the standard framework for galaxy formation.

**Key words:** galaxies: formation — galaxies: clusters — large-scale structures: cosmology: theory — dark matter

## 1 INTRODUCTION

According to the current paradigm galaxies form and reside inside extended cold dark matter (CDM) haloes. One of the ultimate challenges in astrophysics is to obtain a detailed understanding of how galaxies with different properties occupy haloes of different masses. This link between galaxies and dark matter haloes is an imprint of various complicated

physical process related to galaxy formation such as gas cooling, star formation, merging, tidal stripping and heating, and a variety of feedback processes.

One method to investigate the galaxy-dark matter connection is therefore to consider *ab initio* models for galaxy formation, using either numerical simulations (e.g., Katz, Weinberg & Hernquist 1996; Fardal et al. 2001; Pearce et al. 2000; Kay et al. 2002) and/or “semi-analytical” models (e.g., White & Rees 1978; Kauffmann, White & Guiderdoni 1993; Somerville & Primack 1999; Kauffmann et al. 1999; Cole et al. 2000; Benson et al. 2002; van den Bosch 2002).

<sup>★</sup> E-mail: vdbosch@mpa-garching.mpg.de

A downside of this approach, however, is that phenomenological descriptions have to be used to describe a variety of poorly understood physical processes. Consequently, an alternative method has been developed which completely sidesteps the uncertainties related to how galaxies form. This method tries to infer the link between galaxies and dark matter haloes directly from the observed clustering properties of galaxies. Since haloes of different mass and galaxies of different luminosity and type are all clustered differently, there is only a limited amount of possibilities by which one can distribute galaxies over dark matter haloes such that their clustering properties are consistent with observations. The backbone of this approach is the so-called halo model, which views the evolved, non-linear dark matter distribution in terms of its halo building blocks: on strongly non-linear scales the dark matter distribution is given by the actual density distributions of the virialized haloes, while on larger, close-to-linear scales, the dark matter distribution is given by the distribution of virialized haloes (see Cooray & Sheth 2002 for a detailed review). This halo model has become more and more accurate due to the fact that detailed analytical descriptions for the structure and clustering of dark matter haloes have become available (e.g., Navarro, Frenk & White 1997; Moore et al. 1998; Bullock et al. 2001; Mo & White 1996, 2002; Power et al. 2002).

The halo model can be naturally extended to address the bias of *galaxies* by introducing a model for the halo occupation numbers,  $\langle N(M) \rangle$ , which describes how many galaxies on average (with luminosities  $L > L_{\min}$ ) occupy a halo of mass  $M$ . Numerous studies in the past have used these halo occupation number models to investigate how changes in  $\langle N(M) \rangle$  impact on several statistical properties of the galaxy distribution, such as the real-space two- and three-point correlation functions, the power spectrum and bispectrum of galaxies, the galaxy-mass cross correlation function, the pair-wise velocity dispersions, etc. (Seljak 2000; Scoccimarro et al. 2001; White 2001; Berlind & Weinberg 2002; Scranton 2002a; Kang et al. 2002; Marinoni & Hudson 2002; Kochanek et al. 2002). In addition, several studies have confronted these models with data to put constraints on  $\langle N(M) \rangle$  (Jing, Mo & Börner 1998; Peacock & Smith 2000; Marinoni & Hudson 2002; Kochanek et al. 2002; Jing, Börner & Suto 2002; Bullock, Wechsler & Somerville 2002). With large galaxy redshift surveys becoming available, such as the Two-Degree Field Galaxy Redshift Survey (2dFGRS; see Colless et al. 2001) and the Sloan Digital Sky Survey (SDSS, see York et al. 2000), these models can now be confronted with statistical data of unprecedented quality to obtain stringent constraints on the halo occupation numbers, and therewith on both cosmological parameters and galaxy formation models.

In a recent paper, Yang, Mo & van den Bosch (2002; hereafter Paper 1) have taken this approach one step further by considering the derivative of  $\langle N(M) \rangle$  with respect to  $L_{\min}$ . In particular, they introduced the conditional luminosity function (hereafter CLF)  $\Phi(L|M)dL$ , which gives the average number of galaxies with luminosities in the range  $L \pm dL/2$  that reside in haloes of mass  $M$ . The advantage of the CLF over the halo occupation function  $\langle N(M) \rangle$  is that it allows one to address the clustering properties of galaxies *as function of luminosity*. In addition, the CLF yields a direct link between the halo mass function  $n(M)dM$ , which

gives the number of dark matter haloes per comoving volume with masses in the range  $M \pm dM/2$ , and the galaxy luminosity function (hereafter LF)  $\Phi(L)dL$ , which gives the number of galaxies per comoving volume with luminosities in the range  $L \pm dL/2$ , according to

$$\Phi(L) = \int_0^\infty \Phi(L|M) n(M) dM. \quad (1)$$

Therefore,  $\Phi(L|M)$  is not only constrained by the clustering properties of galaxies, as is the case with  $\langle N(M) \rangle$ , but also by the observed galaxy luminosity function. Furthermore, knowledge of  $\Phi(L|M)dL$  allows one to compute the average total luminosity of galaxies in a halo of mass  $M$ ,

$$\langle L \rangle(M) = \int_0^\infty \Phi(L|M) L dL \quad (2)$$

and thus the average mass-to-light ratio as function of halo mass. This  $\langle M/L \rangle(M)$  yields important constraints on galaxy formation models, as it is a direct measure of the halo mass dependence of the galaxy formation efficiency.

In Paper 1 we focussed on the cosmology dependence of the CLF. In this paper, we use data from the 2dFGRS to compute the CLFs of both early and late-type galaxies and compare our results with several semi-analytical models for galaxy formation. It is well known that galaxies of different morphological types have different luminosity functions and different clustering properties. For example, early-type galaxies have higher characteristic luminosities (e.g., Efstathiou, Ellis & Peterson 1988; Loveday et al. 1992) and are more strongly clustered (e.g., Willmer, Da Costa & Pellegrini 1998; Zehavi et al. 2002) than late-type galaxies. The CLFs presented here allow an interpretation of these morphological dependencies in terms of halo occupation numbers, while our comparison with the semi-analytical models links their physical origin to the framework of galaxy formation models.

Throughout this paper we define  $M$  to be the halo mass inside the radius  $R_{180}$  inside of which the average density is 180 times the cosmic mean density, and  $h$  is the Hubble constant in units of  $100 \text{ km s}^{-1} \text{ Mpc}^{-1}$ .

## 2 OBSERVATIONAL CONSTRAINTS

In paper 1 we used data from the 2dFGRS to constrain the CLF of the entire galaxy population. This data set included over 110500 galaxies with  $17.0 < b_J < 19.2$  and  $z < 0.25$ . In this paper we are interested in the CLFs of the early- and late-type galaxies, for which we need separate LFs and separate measurements of the luminosity dependence of the clustering properties.

Madgwick et al. (2002) used a principal component analysis of galaxy spectra taken from the 2dFGRS to obtain a *spectral* classification scheme. They introduced the parameter  $\eta$ , a linear combination of the two most significant principal components, as a galaxy type classification measure. As shown by Madgwick et al. (2002),  $\eta$  follows a bimodal distribution and can be interpreted as a measure for the current star formation rate in each galaxy. Furthermore  $\eta$  is well correlated with *morphological* type (Madgwick 2002). In what follows we adopt the classification suggested by Madgwick et al. and classify galaxies with  $\eta < -1.4$  as

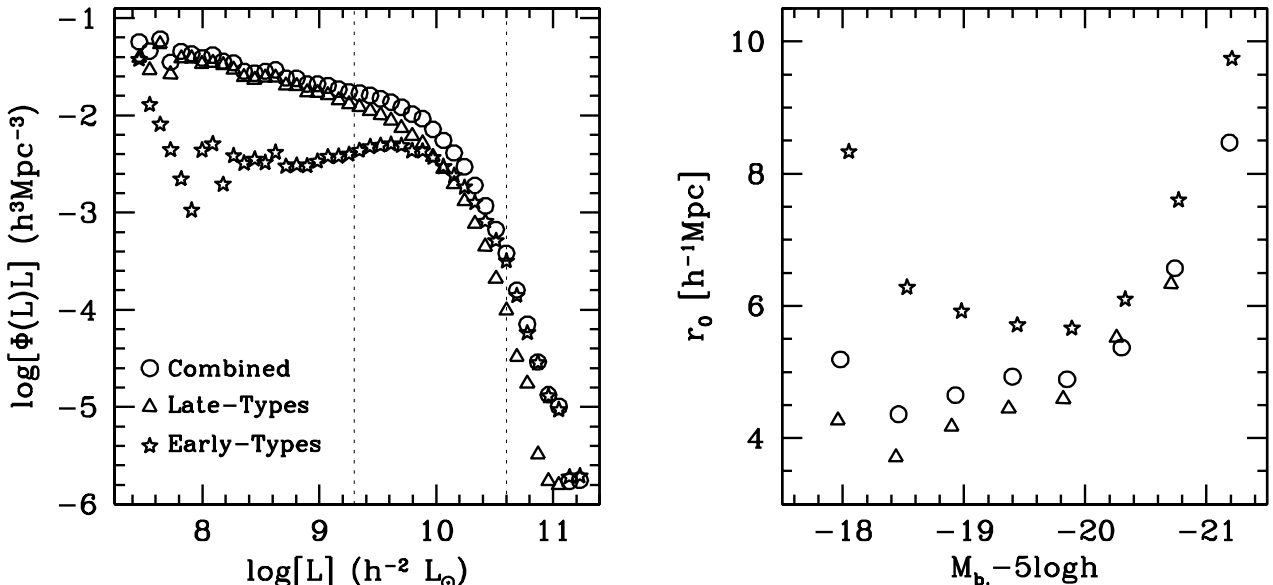


**Figure 1.** The data used to constrain the models. The left panel plots the LFs of the early-type galaxies (starred symbols), the late-type galaxies (open triangles), and the combined sample of late- plus early-type galaxies (open circles). For clarity, no errorbars are shown (but see Figure 2 below). The dotted vertical lines indicate the luminosity range over which measurement of clustering correlation lengths are available. Right panel plots these galaxy-galaxy correlation lengths as function of luminosity (same symbols); Again, for clarity no errorbars are shown (but see Figure 2).

‘early-types’ and galaxies with  $\eta \geq -1.4$  as ‘late-types’. We caution the reader that despite the good correlation between  $\eta$  and morphological type, there is not a one-to-one correspondence between our description of early- and late-type galaxies and those obtained using a more morphological criterion.

## 2.1 Luminosity Functions

In order to constrain the CLFs of early- and late-type galaxies we adopt the LFs in the photometric  $b_J$  band computed by Madgwick et al. (2002) from the 2dFGRS. This sample is restricted to the redshift range  $z \leq 0.15$  and contains 75589 unique galaxies with accurate type-classification based on  $\eta$ . About 36 percent of these galaxies have  $\eta < -1.4$  and make up what we refer to as the sample of early-type galaxies; the remainder makes up the late-type galaxies. In what follows, we shall refer to the *entire* sample (both late- and early-type galaxies) as the “combined sample”.

The LFs obtained from this sample of galaxies have been corrected for completeness effects, and a self-consistent method for  $k$ -corrections, based on the observed 2dF spectra, has been applied. A cosmology with  $\Omega_0 = 0.3$  and  $\Omega_\Lambda = 0.7$  has been adopted, which corresponds to the same cosmological parameters as we adopt throughout this paper.

The left panel of Figure 1 plots the LFs for the combined sample (circles), as well as its contributions from late-type (triangles) and early-type (starred symbols) galaxies. In their paper, Madgwick et al. (2002) subdivided the late-type galaxies in three sub-types. The late-type LF used here is computed by summing the LFs of these three subtypes, and by adding the errors in quadrature. For clarity, no errorbars have been plotted, but these can be seen in Figure 2 below. The main characteristics of these LFs are that (i)

the LFs of the combined and late-type samples are well fit by a Schechter (1976) function (see Madgwick et al. (2002) for the parameters), (ii) early- (late-) type galaxies dominate the total LF at the bright (faint) end, and (iii) the LF of the early-type galaxies reveals a remarkable, though only marginally significant, upturn at the faint-end.

## 2.2 Correlation Lengths

It is straightforward to see that there is an infinite set of CLFs that, given a halo mass function, can reproduce the observed LF  $\Phi_{\text{obs}}(L)$  of galaxies. For example, all CLFs given by  $\Phi(L|M) = [\Phi_{\text{obs}}(L)/n(M_0)]\delta_k(M - M_0)$ , where  $\delta_k(x)$  is the Kronecker delta function and  $M_0$  is an arbitrary mass, yield exactly the same LF, namely  $\Phi_{\text{obs}}(L)$  (see equation [1]). Therefore, in order to constrain the CLF, additional constraints are required. Since more massive dark matter haloes are more strongly clustered (e.g., Mo & White 1996), galaxy-galaxy correlation lengths as function of luminosity,  $r_0(L)$ , put important constraints on how galaxies of different luminosities have to be distributed over haloes of different masses. Indeed, as shown in Paper 1, a combination of an observed LF with measurements of  $r_0(L)$  allow the CLF to be well constrained.

Because of the sheer size of the 2dFGRS it is possible to compute the clustering properties of galaxies of different spectral types and luminosities in representative volume-limited samples. Norberg et al. (2002) obtained real space galaxy-galaxy two-point correlation functions  $\xi_{\text{gg}}(r)$  from the same sample of 2dFGRS galaxies as that used by Madgwick et al. (2002) for the LFs. For a number of volume-limited subsamples (specified by a range in absolute magnitude) Norberg et al. computed  $\xi_{\text{gg}}(r)$  (assuming  $\Omega_0 = 0.3$  and  $\Omega_\Lambda = 0.7$ ) separately for the late-type, the early-type,

and the combined samples. Each of these correlation functions is well fit by a simple power-law  $\xi_{\text{gg}}(r) = (r/r_0)^\gamma$ . Although there is no clear trend of  $\gamma$  with either luminosity or spectral type (see Section 6), the correlation lengths  $r_0$  depend strongly on both luminosity and spectral type. This is shown in the right panel of Figure 1, which plots  $r_0(L)$  for the late-type galaxies (triangles), the early-type galaxies (starred symbols), and the combined sample (circles). For clarity, no errorbars are plotted (but see Figure 2 below). Two trends are apparent: typically  $r_0$  increases with luminosity (i.e., more luminous galaxies are more strongly clustered) and early-type galaxies are more strongly clustered than late-type galaxies of the same luminosity. This type-dependence is particularly strong for the fainter galaxies.

Note that the correlation function itself may also evolve with redshift, an effect that has not been corrected for. For the redshift range covered by the 2dFGRS data used here (i.e.,  $z \leq 0.15$ ), this effect is fairly small, but we nevertheless take it into account in our modeling (see Section 3 below).

### 3 THEORETICAL BACKGROUND

Our main goal in this paper is to use the observed LFs and correlation lengths to constrain the CLFs of the early-type and late-type galaxies. Here we briefly describe how to compute LFs and correlation functions from a given CLF. More details can be found in Paper 1 and references therein.

To compute the galaxy LF  $\Phi(L)$  from the CLF  $\Phi(L|M)$  (equation [1]) one needs the (cosmology-dependent) mass function  $n(M)$  of dark matter haloes, which (at  $z = 0$ ) is given by

$$n(M) \, dM = \frac{\bar{\rho}}{M^2} \nu f(\nu) \left| \frac{d \ln \sigma}{d \ln M} \right| \, dM. \quad (3)$$

Here  $\bar{\rho}$  is the mean matter density of the Universe at  $z = 0$ ,  $\nu = \delta_c/\sigma(M)$ ,  $\delta_c$  is the critical overdensity required for collapse at  $z = 0$ ,  $f(\nu)$  is a function of  $\nu$  to be specified below, and  $\sigma(M)$  is the linear rms mass fluctuation on mass scale  $M$ , which is given by the linear power spectrum of density perturbations  $P(k)$  as

$$\sigma^2(M) = \frac{1}{2\pi^2} \int_0^\infty P(k) \widehat{W}_M^2(k) k^2 \, dk, \quad (4)$$

where  $\widehat{W}_M(k)$  is the Fourier transform of the smoothing filter on mass scale  $M$ .

Throughout we adopt the form of  $f(\nu)$  suggested by Sheth, Mo & Tormen (2001):

$$\nu f(\nu) = 0.644 \left(1 + \frac{1}{\nu^{0.6}}\right) \left(\frac{\nu'^2}{2\pi}\right)^{1/2} \exp\left(-\frac{\nu'^2}{2}\right) \quad (5)$$

with  $\nu' = 0.841 \nu$ . The resulting mass function has been shown to be in excellent agreement with numerical simulations, as long as halo masses are defined as the masses inside a sphere with an average overdensity of about 180 (Sheth & Tormen 1999; Jenkins et al. 2001; White 2002). Therefore, in what follows we consistently use that definition of halo mass, and we use the CDM power spectrum  $P(k)$  of Efstathiou, Bond & White (1992) with a spatial top-hat filter for which

$$\widehat{W}_M(k) = \frac{3}{(kR)^3} [\sin(kR) - kR \cos(kR)] \quad (6)$$

where the mass  $M$  and filter radius  $R$  are related according to  $M = 4\pi\bar{\rho}R^3/3$ .

In order to compute  $r_0(L)$  from the CLF we proceed as follows. In the halo model it is natural to consider the galaxy-galaxy two-point correlation function,  $\xi_{\text{gg}}(r)$ , to be built up from two parts; a 1-halo term,  $\xi_{\text{gg}}^{\text{1h}}(r)$ , which represents the correlation due to pairs of galaxies within the same halo, and a 2-halo term,  $\xi_{\text{gg}}^{\text{2h}}(r)$ , describing the contribution due to pairs of galaxies that occupy different haloes. The observed correlation lengths are all well in excess of  $3.5h^{-1}$  Mpc. At radii this large the contribution from the 1-halo term is negligible and for the purpose of calculating correlation lengths only the 2-halo term is required.

As we show in Appendix A, the 2-halo term of  $\xi_{\text{gg}}(r)$  for galaxies with  $L_1 < L < L_2$  can be written as

$$\xi_{\text{gg}}^{\text{2h}}(r) = \bar{b}^2 \xi_{\text{dm}}^{\text{2h}}(r), \quad (7)$$

with  $\xi_{\text{dm}}^{\text{2h}}(r)$  the 2-halo term of the dark matter mass correlation function at  $z = 0$ , which at scales of the correlation length is well fit by a single power-law

$$\xi_{\text{dm}}^{\text{2h}}(r) \simeq \xi_{\text{dm}}(r) \simeq \left(\frac{r}{r_{0,\text{dm}}}\right)^{-1.75} \quad (8)$$

and

$$\bar{b} = \frac{\int_0^\infty n(M) \langle N(M) \rangle b(M) \, dM}{\int_0^\infty n(M) \langle N(M) \rangle \, dM} \quad (9)$$

Here

$$\langle N(M) \rangle = \int_{L_1}^{L_2} \Phi(L|M) \, dL \quad (10)$$

is the mean number of galaxies in the specified luminosity range for haloes of mass  $M$ , and  $b(M)$  is the bias of dark matter haloes of mass  $M$  with respect to the dark matter mass distribution (see Appendix A). Note that the 2-halo term of the galaxy-galaxy correlation function is completely specified by the CLF and does not require knowledge about how galaxies are distributed inside individual dark matter haloes.

Since  $\bar{b}$  is scale-independent, we can rewrite equation (7) directly in terms of the correlation length for galaxies as

$$r_0 = \bar{b}^{1.143} r_{0,\text{dm}} \quad (11)$$

There is one additional effect, though, that we have to take into account. The correlation functions obtained by Norberg et al. (2002) have not been corrected for possible redshift evolution. This implies that the  $r_0(L)$  measurements do not correspond to  $z = 0$ . In fact, since more luminous galaxies can be detected out to higher redshift, the correlation lengths of brighter galaxies correspond to galaxy populations with a higher median redshift. Therefore, in order to compare model and observations in a consistent way, we have to compute the correlation lengths at the characteristic redshift of the sample in consideration. We take this into account by replacing  $\bar{b}$  in equation (11) with  $\bar{b}_{\text{eff}}(\bar{z})$ . Here  $\bar{z}$  is the mean redshift of the galaxies in consideration (taken from Norberg et al. 2002) and  $\bar{b}_{\text{eff}}$  is the effective bias defined in Appendix B. Since the 2dFGRS sample used here is

limited to  $z \leq 0.15$ , this redshift correction is only modest, amounting to no more than a few percent change in  $r_0$ .

#### 4 MODELING THE CONDITIONAL LUMINOSITY FUNCTION

In Paper 1 we adopted a particular parameterization of the CLF for the entire galaxy population (early plus late type galaxies), and we used a  $\chi^2$  minimization routine to find those parameters that best fit the observed  $\Phi(L)$  and  $r_0(L)$ . Here we seek to constrain two independent CLFs, namely that of the early-type galaxies, hereafter  $\Phi_e(L|M)$ , and that of the late-type galaxies, hereafter  $\Phi_l(L|M)$ . In principle we could use the same parameterizations as in Paper 1 for both of these CLFs independently. However, there is an additional constraint that these CLFs have to fulfill: their sum must be equal to the CLF of the entire galaxy population, and thus be consistent with the  $\Phi(L)$  and  $r_0(L)$  of the combined sample. We therefore use a slightly different, two-step method which automatically obeys the constraint that  $\Phi(L|M) = \Phi_l(L|M) + \Phi_e(L|M)$ . We first use the same method as in Paper 1 to obtain the CLF  $\Phi(L|M)$  of the combined sample (step one). Next we introduce the function  $f_l(L, M)$ , which specifies the late-type fraction of galaxies with luminosity  $L$  in haloes of mass  $M$ . The CLFs of late- and early-type galaxies are then given by

$$\Phi_l(L|M)dL = f_l(L, M) \Phi(L|M)dL \quad (12)$$

and, by definition,

$$\Phi_e(L|M)dL = [1 - f_l(L, M)] \Phi(L|M)dL \quad (13)$$

What remains (step two) is to find the  $f_l(L, M)$  that, given our best-fit CLF for the combined population, best fits the LFs and correlation lengths of the early- and late-type galaxies.

Following Paper 1 we assume that the CLF of the combined sample can be described by a Schechter function:

$$\Phi(L|M)dL = \frac{\tilde{\Phi}^*}{\tilde{L}^*} \left( \frac{L}{\tilde{L}^*} \right)^{\tilde{\alpha}} \exp(-L/\tilde{L}^*) dL \quad (14)$$

Here  $\tilde{L}^* = \tilde{L}^*(M)$ ,  $\tilde{\alpha} = \tilde{\alpha}(M)$  and  $\tilde{\Phi}^* = \tilde{\Phi}^*(M)$ ; i.e., the three parameters that describe the conditional LF depend on  $M$ . In what follows we do not explicitly write this mass dependence, but consider it understood that quantities with a tilde are functions of  $M$ .

We adopt the same parameterizations of these three parameters as in Paper 1, which we repeat here for completeness. Readers interested in the motivations behind these particular choices are referred to Paper 1. For the total mass-to-light ratio of a halo of mass  $M$  we write

$$\left\langle \frac{M}{L} \right\rangle (M) = \frac{1}{2} \left( \frac{M}{L} \right)_0 \left[ \left( \frac{M}{M_c} \right)^{-\gamma_1} + \left( \frac{M}{M_c} \right)^{\gamma_2} \right], \quad (15)$$

which has four free parameters: a characteristic mass  $M_c$ , for which the mass-to-light ratio is equal to  $(M/L)_0$ , and two slopes,  $\gamma_1$  and  $\gamma_2$ , which specify the behavior of  $\langle M/L \rangle$  at the low and high mass ends, respectively. A similar parameterization is used for the characteristic luminosity  $\tilde{L}^*$ :

$$\frac{M}{\tilde{L}^*(M)} = \frac{1}{2} \left( \frac{M}{L} \right)_0 f(\tilde{\alpha}) \left[ \left( \frac{M}{M_c} \right)^{-\gamma_1} + \left( \frac{M}{M_2} \right)^{\gamma_3} \right]. \quad (16)$$

Here

$$f(\tilde{\alpha}) = \frac{\Gamma(\tilde{\alpha} + 2)}{\Gamma(\tilde{\alpha} + 1, 1)}. \quad (17)$$

with  $\Gamma(x)$  the Gamma function and  $\Gamma(a, x)$  the incomplete Gamma function. This parameterization has two additional free parameters: a characteristic mass  $M_2$  and a power-law slope  $\gamma_3$ . For  $\tilde{\alpha}(M)$  we adopt:

$$\tilde{\alpha}(M) = \alpha_{15} + \zeta \log(M_{15}). \quad (18)$$

Here  $M_{15}$  is the halo mass in units of  $10^{15} h^{-1} M_\odot$ ,  $\alpha_{15} = \tilde{\alpha}(M_{15} = 1)$ , and  $\zeta$  describes the change of the faint-end slope  $\tilde{\alpha}$  with halo mass. Note that once  $\tilde{\alpha}$  and  $\tilde{L}^*$  are given, the normalization  $\tilde{\Phi}^*$  of the CLF is obtained through equation (15), using the fact that the total (average) luminosity in a halo of mass  $M$  is given by

$$\langle L \rangle (M) = \int_0^\infty \Phi(L|M) L dL = \tilde{\Phi}^* \tilde{L}^* \Gamma(\tilde{\alpha} + 2). \quad (19)$$

Finally, we introduce the mass scale  $M_{\min}$  below which the CLF is zero; i.e., we assume that no stars form inside haloes with  $M < M_{\min}$ . Motivated by reionization considerations (see Paper 1 for details) we adopt  $M_{\min} = 10^9 h^{-1} M_\odot$  throughout. This lower-mass limit does not significantly influence our results. For instance, changing  $M_{\min}$  to either  $10^8 h^{-1} M_\odot$  or  $10^{10} h^{-1} M_\odot$  has only a very modest impact on the results presented below.

In order to split the CLF in early- and late-type galaxies we make the assumption that  $f_l(L, M)$  has a quasi-separable form

$$f_l(L, M) = g(L) h(M) q(L, M) \quad (20)$$

Here

$$q(L, M) = \begin{cases} 1 & \text{if } g(L) h(M) \leq 1 \\ \frac{1}{g(L) h(M)} & \text{if } g(L) h(M) > 1 \end{cases} \quad (21)$$

is to ensure that  $f_l(L, M) \leq 1$ . For the  $g(L)$  and  $h(M)$  adopted here (see below),  $q(L, M) = 1$  for the vast majority of the relevant  $(L, M)$  parameter space, and therefore  $f_l(L, M)$  can be considered separable to good accuracy. This basically implies that the *shapes* (but not the absolute values) of the conditionals  $f_l(L|M)$  and  $f_l(M|L)$  are independent of  $M$  and  $L$ , respectively. Note that  $g(L)$  is not the same as the fraction  $\mathcal{F}_l(L)$  of all galaxies with luminosity  $L$  that are late-type, which instead is given by

$$\mathcal{F}_l(L) = \frac{\Phi_l(L)}{\Phi(L)} = \frac{\int_0^\infty f_l(L, M) \Phi(L|M) n(M) dM}{\int_0^\infty \Phi(L|M) n(M) dM} \quad (22)$$

Similarly, the fraction of all galaxies in haloes of mass  $M$  that are late-type is given by

$$\mathcal{F}_l(M) = \frac{\int_0^\infty f_l(L, M) \Phi(L|M) dL}{\int_0^\infty \Phi(L|M) dL} \quad (23)$$

The challenge now is to find the  $g(L)$  and  $h(M)$  that, given the CLF for the combined sample, reproduce the observed LFs and  $r_0(L)$  of the early- and late-type galaxies. To achieve this we use the following estimate for  $g(L)$ :

$$g(L) = \frac{\hat{\Phi}_l(L)}{\hat{\Phi}(L)} \frac{\int_0^\infty \Phi(L|M) n(M) dM}{\int_0^\infty \Phi(L|M) h(M) n(M) dM} \quad (24)$$

where  $\hat{\Phi}_l(L)$  and  $\hat{\Phi}(L)$  correspond to the *observed* LFs of the late-type and combined galaxy samples, respectively. For any  $L$  for which  $f_l(L, M)$  is separable (i.e., for which  $q(L, M) = 1$  for all  $M$ ), this implies that the LFs of the early- and late-type galaxies are given by

$$\Phi_{e,l}(L) = \hat{\Phi}_{e,l}(L) \frac{\Phi(L)}{\hat{\Phi}(L)}, \quad (25)$$

i.e., as long as the observed LF of the combined sample is well fit by the model, the same will be true for the LFs of the early- and late-type galaxies. For the  $L$  for which  $q(L, M) < 1$  a (typically small) correction to (25) applies. What remains is to find the  $h(M)$  that best reproduces the  $r_0(L)$  of the early- and late-type galaxies. This requires the average biases  $\bar{b}_l$  and  $\bar{b}_e$  for late- and early-type galaxies, respectively, which are obtained from equations (9) and (10) by replacing  $\Phi(L|M)$  with  $\Phi_l(L|M)$  and  $\Phi_e(L|M)$ , respectively.

After experimenting with a variety of different functional forms for  $h(M)$  we finally decided to adopt

$$h(M) = \max \left( 0, \min \left[ 1, \left( \frac{\log(M/M_0)}{\log(M_1/M_0)} \right) \right] \right) \quad (26)$$

Here  $M_0$  and  $M_1$  are two free parameters, defined as the masses at which  $h(M)$  takes on the values 0 and 1, respectively. Note that both  $h(M)$  and  $g(L)$  can in principle take on any positive value. However, for computational reasons we limit  $h(M)$  to take values in the range  $[0, 1]$ . This does not impact our results, as any linear scaling of  $h(M)$  reflects itself in  $g(L)$  through equation (24).

Our model for the three CLFs thus contains a total of 10 free parameters: 4 characteristic masses;  $M_c$ ,  $M_0$ ,  $M_1$  and  $M_2$ , four parameters that describe the various mass-dependencies  $\gamma_1$ ,  $\gamma_2$ ,  $\gamma_3$  and  $\zeta$ , and 2 normalizations; one for the mass-to-light ratio,  $(M/L)_0$ , and one for the faint-end slope of the CLF,  $\alpha_{15}$ . Although this may seem an awful lot, it is important to realize that we use this model to fit 67 independent data points<sup>†</sup>. Furthermore, as we show in Section 5 below one can actually use observational constraints to fix several of these free parameters. In addition, the data is of sufficient quality to constrain the model freedom. Alternatively, we could have chosen a more restrictive (with fewer free parameters) form for the CLFs, but lacking both observational and physical motivations for a more preferred form of the CLF we felt the need to be sufficiently general. On the other side, one might argue that because of this lack, our model is actually too constrained. For instance, the fact that we assume a Schechter function for the CLF is at best weakly motivated by the observed LFs of clusters of galaxies (e.g., Muriel, Valotto & Lambas 1998; Beijersbergen et al. 2002; Trentham & Hodgkin 2002; Martínez et al. 2002). However, as we show below, our model can accurately fit all observations. Therefore, the use of more general models would only result in a larger amount of degeneracy and will therefore have to await more stringent constraints from either the SDSS or the completed 2dFGRS.

<sup>†</sup> Because of our definition of  $g(L)$  only 67 of the in total 155 data points are independent.

## 5 RESULTS

The cosmological model sets the halo mass function  $n(M)dM$ , the dark matter two-point correlation function  $\xi_{dm}(r)$ , and the halo bias function  $b(M)$ . Therefore, different cosmologies imply different halo occupancy functions. In this paper we focus on the  $\Lambda$ CDM cosmology with  $\Omega_0 = 0.3$ ,  $\Omega_\Lambda = 0.7$ ,  $h = 0.7$ ,  $\Gamma = \Omega_0 h = 0.21$ , and  $\sigma_8 = 0.9$ . These cosmological parameters are consistent with recent measurements of the cosmic microwave background (e.g., Pryke et al. 2001) and large scale structure measurements (e.g., Tegmark, Hamilton & Xu 2002). In addition, we have shown in Paper 1 that this cosmology is also the most successful in explaining the LF and galaxy clustering luminosity dependence observed. Therefore, in what follows, we restrict ourselves to this ‘‘concordance’’ cosmology.

Having specified our model, the observational constraints, and the cosmological parameters, we now proceed as follows. We first use Powell’s multi-dimensional direction set method (e.g., Press et al. 1992) to find the parameters of the CLF of the combined sample that minimize

$$\chi^2 = \frac{\chi^2(\Phi)}{N_\Phi} + \frac{\chi^2(r_0)}{N_r}. \quad (27)$$

Here

$$\chi^2(\Phi) = \sum_{i=1}^{N_\Phi} \left[ \frac{\Phi(L_i) - \hat{\Phi}(L_i)}{\Delta \hat{\Phi}(L_i)} \right]^2, \quad (28)$$

and

$$\chi^2(r_0) = \sum_{i=1}^{N_r} \left[ \frac{r_0(L_i) - \hat{r}_0(L_i)}{\Delta \hat{r}_0(L_i)} \right]^2, \quad (29)$$

with  $\hat{\Phi}(L_i)$  and  $\hat{r}_0(L_i)$  the observed values, and  $N_\Phi = 44$  and  $N_r = 8$  the number of corresponding data points.

Note that the scaling of  $\chi^2$  with  $N_\Phi$  and  $N_r$  implies that we assign equal weights to  $\chi^2(\Phi)$  and  $\chi^2(r_0)$ . This differs from the proper statistical  $\chi^2$  for which each individual *measurement* should receive equal weights. However, since  $N_\Phi > N_r$  and since the errors on  $\hat{\Phi}(L)$  are typically much smaller than the errors on  $\hat{r}_0(L)$ , the  $\chi^2$  minimization routine would give much more weight to fitting the LF than to fitting the correlation lengths. Note that the proper  $\chi^2$  is only well defined if there are no systematic errors in the measurements and if the error properties of  $\hat{\Phi}(L)$  and  $\hat{r}_0(L)$  are the same. It is unlikely that these requirements are fulfilled, and our modified  $\chi^2$  is therefore equally meaningful as that of the proper  $\chi^2$ .

We start our investigation using all available model freedom, which means that we minimize  $\chi^2$  over a total of 10 free parameters. In the first step we find the 8 parameters of the CLF that best fits the LF and correlation lengths of the combined sample. In the second step, we then find the  $M_0$  and  $M_1$ , describing  $h(M)$ , that best reproduce the observed clustering properties of the early- and late-type galaxies. We refer to this model with maximum freedom as model A.

The resulting best-fit parameters are listed in Table 1, and the fits to the data are shown in the upper panels of Figure 2 (solid lines). Overall the fit to the data is remarkably good. The fact that the model reproduces even the small scale features in the LF of the early-type galaxies is a direct

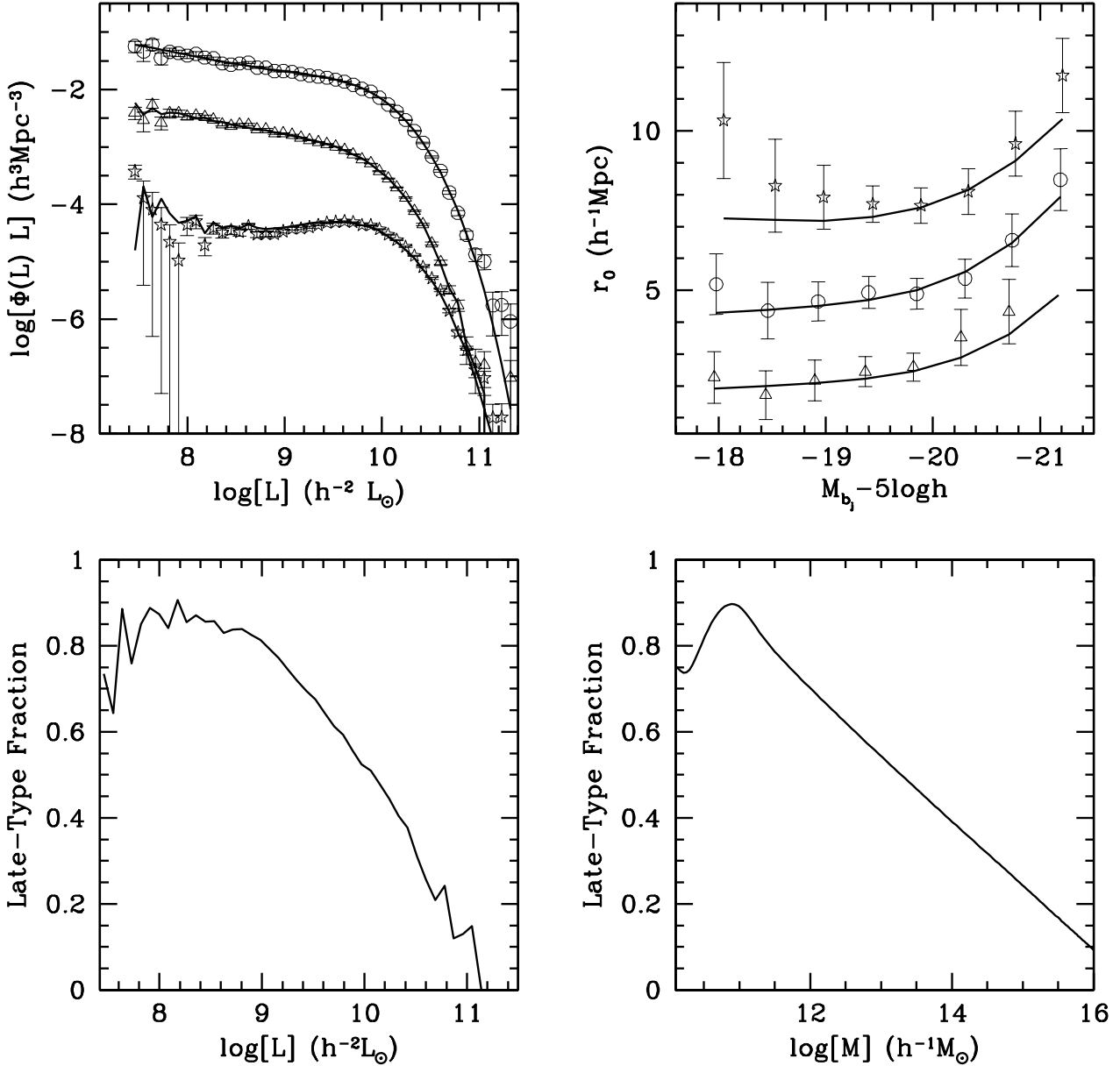


**Figure 2.** Results for model A. The upper two panels plot the observed LFs (left panel) and correlation lengths (right panel). Symbols are the same as in Figure 1, while the solid lines indicate the model results. For clarity, the LFs have been separated from each other by one order of magnitude in the  $y$ -direction, with the combined LF untranslated. Similarly, the  $r_0(L)$  of the early- and late-type galaxies are offset by  $+2h^{-1}$  Mpc and  $-2h^{-1}$  Mpc, respectively. Note the good quality of the fits. The lower panels plot the fraction of late-type galaxies as function of luminosity (left) and halo mass (right).

consequence of the way in which we have defined  $g(L)$  (see Section 4).

The lower two panels of Figure 2 plot the number fractions of late-type galaxies as function of luminosity,  $\mathcal{F}_l(L)$ , and mass,  $\mathcal{F}_l(M)$ . The fraction of late-type galaxies decreases with both increasing luminosity and mass. Note that this is, at least qualitatively, in agreement with the well-known morphology-density relation. The ‘noisy’ wiggles in  $\mathcal{F}_l(L)$  are due to the fact that  $g(L)$  is computed directly from the observed LFs, while the feature in  $\mathcal{F}_l(M)$  for  $M \lesssim 3 \times 10^{10} h^{-1} M_\odot$  is a consequence of the upturn in the LF of early-type galaxies at  $L \lesssim 10^8 h^{-2} L_\odot$ .

The upper-right panel of Figure 3 plots the total, av-

erage mass-to-light ratio of model A as function of halo mass, computed using equation (2). The  $\langle M/L \rangle(M)$  reveals a sharp minimum of  $\sim 110 h(M/L)_\odot$  at  $M \simeq 2 \times 10^{11} h^{-1} M_\odot$ . For  $M < 2 \times 10^{11} h^{-1} M_\odot$  the mass-to-light ratios increase dramatically with decreasing mass, such that in haloes with  $M \lesssim 10^{10} h^{-1} M_\odot$  virtually no (blue) light is produced. This sharp increase of  $\langle M/L \rangle$  with decreasing halo mass is required in order to bring the steep slope of the halo mass function at low  $M$  in agreement with the relatively shallow faint-end slope of the observed LF. In the language of galaxy formation models; low-mass haloes need efficient feedback to prevent an overabundance of faint galaxies. For haloes with  $M > 2 \times 10^{11} h^{-1} M_\odot$  the (average) mass-to-light ratio

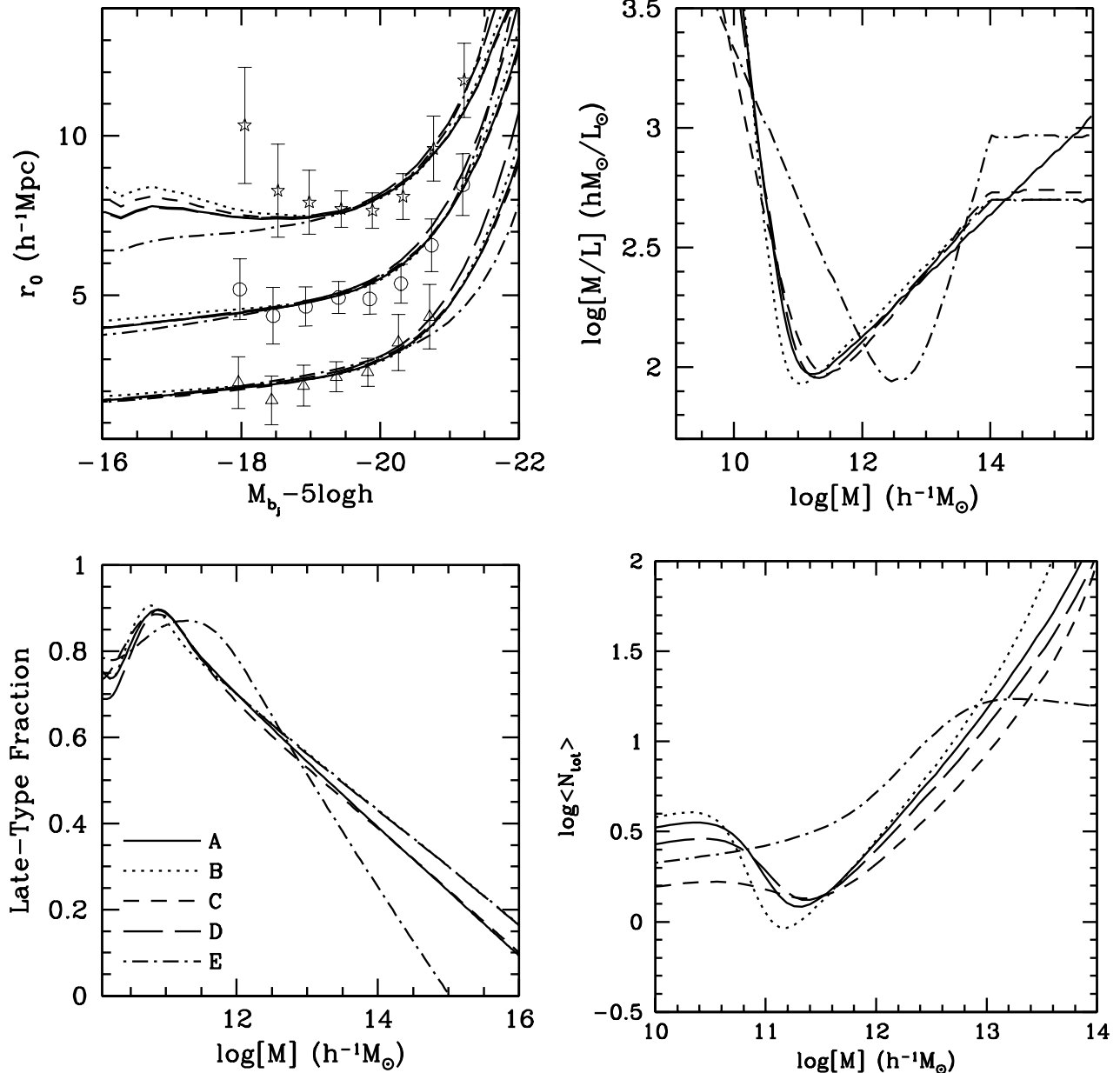


**Figure 3.** A comparison of the five models discussed in the text. The upper panel on the left plots the correlation lengths as function of luminosity. Symbols with errorbars correspond to the 2dFGRS data with the  $r_0(L)$  of the late-type and early-type galaxies translated by  $-2h^{-1}$  Mpc and  $+2h^{-1}$  Mpc, respectively. The fits of these models to the observed LFs are not shown, since the differences between the various models can not be discerned by eye. The other three panels plot, for all five models, the inferred mass-to-light ratios  $\langle M/L \rangle(M)$  (upper right), the late-type fractions  $\mathcal{F}_l(M)$  (lower left) and the average total number of galaxies  $\langle N_{\text{tot}}(M) \rangle$  (lower right). Model E predicts mass-to-light ratios and late-type fractions for cluster-sized haloes that are inconsistent with data. In order to discriminate between the other models, better constraints on  $r_0$  for faint, early-type galaxies and/or accurate, independent measurements of  $\mathcal{F}_l(M)$  and/or  $\langle M/L \rangle$  for haloes with  $M \gtrsim 10^{14}h^{-1}\text{M}_\odot$  are required.

increases roughly as  $\langle M/L \rangle \propto M^{0.3}$ , such that clusters of  $10^{15}h^{-1}\text{M}_\odot$  have, on average, a (blue) mass-to-light ratio of  $\sim 1000h\langle M/L \rangle_\odot$ . Within the context of galaxy formation models, this increase in mass-to-light ratio is interpreted as a decrease of the cooling efficiency in more massive haloes (e.g., White & Rees 1978; White & Frenk 1991).

By construction,  $\langle M/L \rangle \propto M^{\gamma_2}$  for haloes with  $M \gg M_c$ . However, several studies have suggested that on cluster mass scales  $\langle M/L \rangle$  varies only weakly with mass (e.g., Bah-

call, Lubin & Norman 1995; Bahcall et al. 2000; Kochanek et al. 2002). Furthermore, Fukugita, Hogan & Peebles (1998), using a variety of observational constraints, derived that clusters of galaxies have blue mass-to-light ratios of  $450 \pm 100h\langle M/L \rangle_\odot$ , i.e., more than  $5\sigma$  lower than what model A predicts for a Coma sized cluster. Therefore, we now consider a model (model B) in which we keep  $\langle M/L \rangle$  fixed at a constant value of  $\langle M/L \rangle_{\text{cl}}$  for haloes with  $M \geq 10^{14}h^{-1}\text{M}_\odot$ . Motivated by Fukugita et al. (1998) we adopt  $\langle M/L \rangle_{\text{cl}} =$

**Table 1.** Model parameters.

| ID<br>(1) | $\log M_L$<br>(2) | $(M/L)_{cl}$<br>(3) | $\log M_c$<br>(4) | $\log M_0$<br>(5) | $\log M_1$<br>(6) | $\log M_2$<br>(7) | $(M/L)_0$<br>(8) | $\gamma_1$<br>(9) | $\gamma_2$<br>(10) | $\gamma_3$<br>(11) | $\zeta$<br>(12) | $\alpha_{15}$<br>(13) | $\chi^2(\Phi)$<br>(14) | $\chi^2(r_0)$<br>(15) |
|-----------|-------------------|---------------------|-------------------|-------------------|-------------------|-------------------|------------------|-------------------|--------------------|--------------------|-----------------|-----------------------|------------------------|-----------------------|
| A         | 13.20             | —                   | 10.85             | 16.64             | 8.60              | 12.15             | 136              | 2.35              | 0.26               | 0.73               | -0.19           | -1.09                 | 65.0                   | 5.8                   |
| B         | 13.03             | <b>500</b>          | 10.72             | 17.27             | 7.92              | 12.21             | 128              | 3.04              | 0.27               | 0.73               | -0.19           | -1.20                 | 64.6                   | 5.2                   |
| C         | <b>13.25</b>      | 544                 | 11.11             | 16.71             | 8.83              | 11.82             | 115              | 1.36              | 0.34               | 0.65               | -0.39           | -1.27                 | 64.7                   | 5.6                   |
| D         | <b>13.25</b>      | <b>500</b>          | 10.94             | 17.26             | 10.86             | 12.04             | 124              | 2.02              | 0.30               | 0.72               | -0.22           | -1.10                 | 64.3                   | 5.4                   |
| E         | <b>13.50</b>      | 924                 | 12.67             | 15.02             | 10.11             | 11.60             | 89               | 0.63              | 0.99               | 0.69               | -0.20           | -0.73                 | 71.0                   | 6.3                   |
| B1        | 13.03             | <b>500</b>          | 10.72             | <b>17.00</b>      | <b>12.00</b>      | 12.21             | 128              | 3.04              | 0.27               | 0.73               | -0.19           | -1.20                 | 64.6                   | 5.4                   |
| B2        | 13.03             | <b>500</b>          | 10.72             | <b>15.00</b>      | <b>13.90</b>      | 12.21             | 128              | 3.04              | 0.27               | 0.73               | -0.19           | -1.20                 | 64.6                   | 5.6                   |

Column (1) lists the ID by which we refer to each model in the text. Columns (2) to (13) list the best-fit model parameters, where parameters that were kept fixed during the fitting procedure are type-set in boldface. Here  $M_L$  is defined such that  $\bar{L}^*(M_L) = L^*$  (see Section 5),  $(M/L)_{cl}$  is the mass-to-light ratio of haloes with  $M \geq 10^{14} h^{-1} M_\odot$ , and  $\alpha_{15}$  is the faint-end slope of the conditional LF for haloes with  $M = 10^{15} h^{-1} M_\odot$ . Columns (14) and (15) list the values of  $\chi^2(\Phi)$  and  $\chi^2(r_0)$  of the best-fit model, respectively. Here  $\chi^2(\Phi)$  corresponds to the  $\chi^2$  of the fit to the LF of the combined sample only ( $N_\Phi = 44$ ), whereas  $\chi^2(r_0)$  is summed over all  $r_0$  measurements of all three samples (combined, early- and late-type;  $N_r = 23$ ). Masses and mass-to-light ratios are in  $h^{-1} M_\odot$  and  $h (M/L)_\odot$ , respectively.

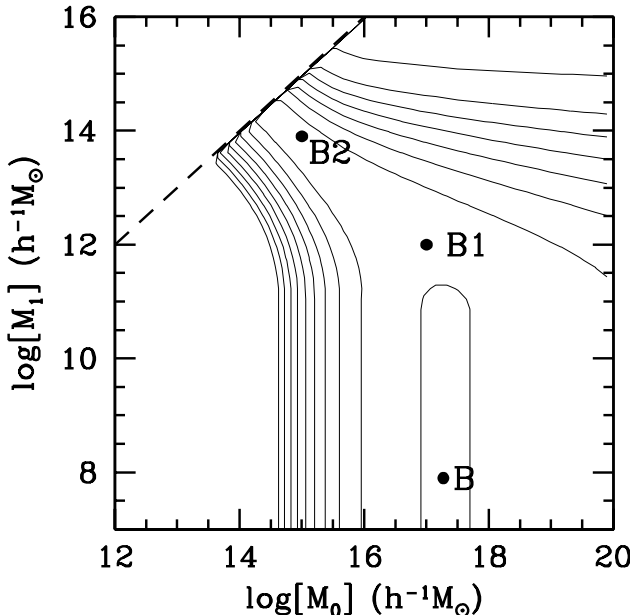


**Figure 4.** Contour plot of  $\chi^2(r_0)$  as function of  $M_0$  and  $M_1$  for model B. Contours correspond to  $\chi^2(r_0) = 5.5, 6.5, 7.5, \dots, 14.5$ . The location of the best-fit model is indicated by a thick dot labeled ‘B’. The locations of models B1 and B2, discussed in the text, are also indicated. The dashed, diagonal line corresponds to  $M_0 = M_1$  and indicates the boundary above which no good fits can be obtained. For models with  $M_1 < M_0$  there is a large area in  $(M_0, M_1)$  parameter space that yields virtually identical  $\chi^2(r_0)$ .

500h  $(M/L)_\odot$ . Continuity of  $\langle M/L \rangle(M)$  then sets the parameter  $\gamma_2$  which is therefore no longer a free parameter. With respect to model A, the minimum of  $\langle M/L \rangle(M)$  occurs at a somewhat lower mass of  $\sim 10^{11} h^{-1} M_\odot$ , the fraction of late-type galaxies in massive haloes has increased, and the fit to the correlation lengths has improved, especially for the faint early-type galaxies (see Figure 3). This is easy to understand: Lowering the mass-to-light ratios on cluster scales means that more galaxies have to reside in clusters. Since more massive haloes are more strongly clustered

(Mo & White 1996) and the majority of cluster galaxies are early-types, this leads to an increase of  $r_0$  which is most pronounced for the early-types.

Although overall model B is in better agreement with the data than model A, it also has an unattractive feature. This is illustrated in the lower right panel of Figure 3 where we plot the average, total number of galaxies

$$\langle N_{\text{tot}}(M) \rangle = \int_0^\infty \Phi(L|M) dL = \tilde{\Phi}^* \Gamma(\tilde{\alpha} + 1) \quad (30)$$

as function of halo mass. Model B predicts that this number is less than unity for haloes with masses around  $10^{11} h^{-1} M_\odot$ . Yet, this mass scale coincides with the *minimum* of  $\langle M/L \rangle(M)$ . This implies that these haloes must have an extremely large spread in  $M/L$ ; the majority of haloes contain zero galaxies (or only “dark” galaxies, which produce no light), while a small fraction harbors one (or more) relatively bright galaxy (in order to explain the  $\langle M/L \rangle$ ). This aspect of the model is due to the fact that the CLF for haloes of this mass scale has a relatively high characteristic luminosity  $\tilde{L}^*$ . If we define  $M_L$  as the mass for which  $\bar{L}^*(M) = L^*$ , where  $L^* = 1.1 \times 10^{10} h^{-2} L_\odot$  is the characteristic luminosity of the *observed* LF of the combined sample (see Madgwick et al. 2002), we find for model B a relatively low value of  $M_L \simeq 10^{13} h^{-1} M_\odot$  (see Table 1). Since the abundance of haloes with this mass is relatively high, reproducing the observed abundance of  $L^*$  galaxies requires a significant fraction of haloes with dark or no galaxies. Although the existence of dark galaxies is interesting in itself (see Verde, Oh & Jimenez 2002), a large scatter in  $M/L$  for haloes with  $M \simeq 10^{11} h^{-1} M_\odot$  seems inconsistent with the small scatter in the observed Tully-Fisher and Fundamental Plane relations (see also discussion in Paper 1).

Therefore, in models C and E we tune the value of  $M_2$  such that  $M_L = 10^{13.25} h^{-1} M_\odot$  and  $10^{13.5} h^{-1} M_\odot$ , respectively (i.e.,  $M_2$  is not a free parameter here). We again set  $M/L$  constant for haloes with  $M \geq 10^{14} h^{-1} M_\odot$ , but we let the value of  $(M/L)_{cl}$  be a free parameter. These models thus have the same number of free parameters as model B. As can be seen from Figure 3, model C is remarkably similar to model A. This is mainly due to the fact that the value of  $M_L$  of model A is with  $10^{13.26}$  close to that of

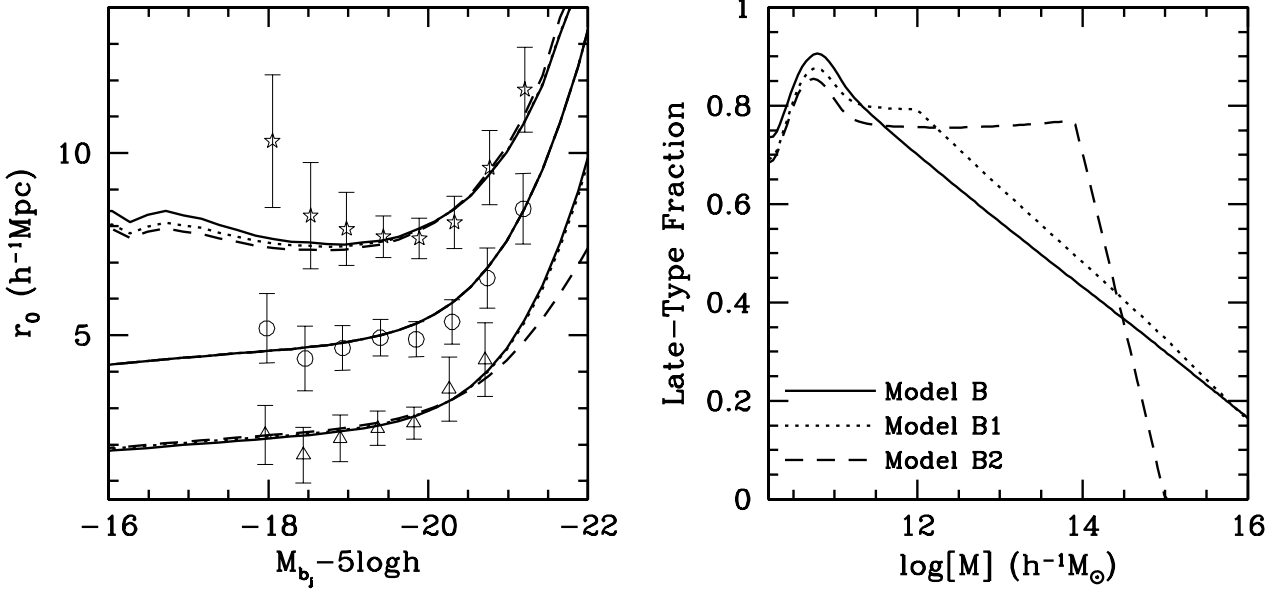


**Figure 5.** Correlation lengths and late-type fractions as function of magnitude and halo mass, respectively, for models B, B1, and B2. Although these three models yield virtually indistinguishable  $r_0(L)$ , they imply  $\mathcal{F}_l(M)$  that are quite different. Note that model B2 can be rejected based on its prediction of zero late-type galaxies in haloes with  $M > 10^{15} h^{-1} M_\odot$ .

model C (see Table 1). The best-fit value of  $(M/L)_{\text{cl}}$  is with  $615h(M/L)_\odot$  consistent with the value advocated by Fukugita et al. (1998) at the  $2\sigma$  level. Model E, however, is dramatically different. The minimum of  $\langle M/L \rangle(M)$  occurs at a significantly higher mass scale of  $\sim 2.5 \times 10^{12} h^{-1} M_\odot$ . In addition,  $(M/L)_{\text{cl}} \simeq 1000h(M/L)_\odot$  and  $\mathcal{F}_l = 0$  for haloes with  $M \gtrsim 10^{15} h^{-1} M_\odot$ , both of which are inconsistent with observations. Furthermore, model E yields a significantly poorer fit to the observed correlation lengths of the faint early-type galaxies, and we therefore no longer consider model E in what follows.

Finally, in model D, we combine the constraints from models B and C above; model D has therefore only 8 free parameters together with  $M_L = 10^{13.25} h^{-1} M_\odot$  and  $(M/L)_{\text{cl}} = 500h(M/L)_\odot$ . With respect to model C this causes a small increase in correlation lengths (again because more light is added to the strongly clustered massive haloes), though the effect is sufficiently small that model D can still be considered as yielding an overall good fit.

Figure 4 plots contours of constant  $\chi^2(r_0)$  in the  $M_0$  versus  $M_1$  plane for model B (results for the other models discussed above are very similar). The dashed diagonal line corresponds to  $M_0 = M_1$  (i.e.,  $h(M)$  is a step-function). Clearly, models with  $M_0 < M_1$  (for which the fraction of late-type galaxies *increases* with halo mass) result in poor fits as the value of  $\chi^2(r_0)$  is always extremely large. This is easy to understand. Since the correlation lengths of the late-type galaxies are smaller than those of the early-type galaxies, and since more massive haloes are more strongly clustered, reproducing the observed  $r_0(L)$  requires that the late-type fraction decreases with halo mass, and thus that  $M_0 > M_1$ . However, as is also apparent from the contour plot, a large area in the  $M_0$ - $M_1$  plane yields roughly equally good fits. To illustrate this “degeneracy” we have also computed two additional models, B1 and B2, for which we keep all parameters identical to that of model B, but we modify

$M_0$  and  $M_1$  so that these models fall in the region of roughly the same  $\chi^2(r_0)$  (indicated by solid dots in Figure 4). Note that changes in  $h(M)$  only affect the  $r_0(L)$  of the early- and late-type galaxies; all LFs and the correlation lengths of the combined sample are unaffected. The results for models B1 and B2 are shown in Figure 5. As is also apparent from their values of  $\chi^2(r_0)$  listed in Table 1, these models are virtually indistinguishable from model B and from each other. However, they do yield somewhat different  $\mathcal{F}_l(M)$ . Model B2 for instance yields late-type fractions of zero for  $M \gtrsim 10^{15} h^{-1} M_\odot$ . This is inconsistent with data, which allows us to rule against this particular model. However, models B1 and B have quite similar  $\mathcal{F}_l(M)$ , and current data is not sufficient to discriminate between these two alternatives. This degeneracy also explains why we have adopted a fairly simple form for  $h(M)$ ; more complicated forms, with more free parameters, only increases the amount of degeneracy.

Having shown that there are different models that fit the data roughly equally well, the question arises whether one can discriminate between these different halo occupancy models. Based on the observed mass-to-light ratios of clusters, and on the amount of scatter inferred from the Tully-Fisher and Fundamental Plane relations, one might argue that of the models presented above, model C is to be preferred (modulo some uncertainties in  $M_0$  and  $M_1$ ). In what follows, however, we always compare predictions from different models. This gives an idea about the extent of the uncertainties in the models, and the accuracy in the data required to allow to discriminate between the various models. Some clues are already apparent from Figure 3. As we have shown above, the models are extremely sensitive to the exact value of  $M_L$  and most of the uncertainties in the models can be translated to values of  $M_L$  in the range  $10^{13} h^{-1} M_\odot$  to  $10^{13.5} h^{-1} M_\odot$ . In order to further constrain this crucial parameter more accurate measurements are required of the

mass-to-light ratios and late-type fractions in clusters or of the correlation lengths of galaxies with  $M_{b_J} - 5\log h \gtrsim -18$ .

In summary, within the concordance cosmology several models can be found that fit the data remarkably well. Although some amount of degeneracy exists, the mean trends reveal an average mass-to-light which has a minimum of  $\sim 100 h (\text{M/L})_{\odot}$  at around  $3 \times 10^{11} h^{-1} \text{M}_{\odot}$ , and which increases extremely rapidly towards lower masses: in all cases we find  $\langle M/L \rangle > 3000 h (\text{M/L})_{\odot}$  for haloes with  $M < 10^{10} h^{-1} \text{M}_{\odot}$ . The correlation lengths require that the fraction of late-type galaxies decreases from about 90 percent for haloes with  $M \lesssim 10^{12} h^{-1} \text{M}_{\odot}$  to anywhere between 0 and 40 percent on scales of  $M = 10^{15} h^{-1} \text{M}_{\odot}$ , in qualitative agreement with the morphology-density relation. Similarly, the observed LFs indicate a similar trend with luminosity: about 90 percent of all galaxies with  $L \lesssim 10^9 h^{-2} \text{L}_{\odot}$  are late-types, while this drops to about 20-30 percent for galaxies brighter than  $L^*$ .

## 6 TWO POINT CORRELATION FUNCTIONS

Two point correlation functions are a powerful tool to describe the clustering properties of galaxies. With the CLFs for early- and late-type galaxies we can compute the galaxy-galaxy correlation function,  $\xi_{gg}(r)$ , not only as function of galaxy type, but also as function of luminosity. This allows a detailed investigation of the bias of galaxies as function of scale, luminosity, and (spectral) type.

At small scales, where the number of pairs are mostly due to galaxies within the same halo,  $\xi_{gg}(r)$  depends not only on the occupation numbers of galaxies (which can be obtained from the CLF), but also on how galaxies are distributed inside individual dark matter haloes. In addition, since the number of pairs within a halo containing  $N$  galaxies is equal to  $\frac{1}{2}N(N-1)$  one also needs to know the second moment of the halo occupation number distribution. Since the CLF only contains information about the first moments  $\langle N(M) \rangle$  we need to make additional assumptions. Alternatively, as shown by Cooray (2002), one may use the observed power spectrum of galaxies to obtain constraints on the second moments of  $P(N|M)$  using standard inversion techniques.

We follow Yang et al. (2002) and make the assumption that the probability distribution  $P(N|M)$ , with  $N$  an integer, is given by

$$P(N|M) = \begin{cases} N' + 1 - \langle N(M) \rangle & \text{if } N = N' \\ \langle N(M) \rangle - N' & \text{if } N = N' + 1 \\ 0 & \text{otherwise} \end{cases} \quad (31)$$

Here  $N'$  is the integer of  $\langle N(M) \rangle$ . Thus, the actual, integer number of galaxies in a halo of mass  $M$  is either  $N'$  or  $N'+1$ . This particular model for the distribution of halo occupation numbers is supported by the semi-analytical models of Benson et al. (2000) who found that the halo occupation probability distribution is narrower than a Poisson distribution. In addition, they have shown that distribution (31), which they call the “average” distribution, is successful in yielding power-law correlation functions, much more so than for example a Poisson distribution (see also Berlind & Weinberg 2002). For this “average” distribution the average number of

galaxy pairs inside an individual dark matter halo is given by

$$\langle N_{\text{pair}}(M) \rangle = N' \langle N(M) \rangle - \frac{1}{2}N' (N' + 1) \quad (32)$$

For the spatial distribution of galaxies within a halo we follow Peacock & Smith (2000), Benson et al. (2000) and Berlind & Weinberg (2002) and assume that (i) the brightest galaxy resides in the center, and (ii) the remaining ‘satellite’ galaxies follow the density distribution of the dark matter (which we specify in Appendix A). The special treatment of a central galaxy is required if the galaxy-galaxy correlation function is to remain close to a single power-law, rather than to reveal a flattening as present in the dark matter mass correlation function (Peacock & Smith 2000; Berlind & Weinberg 2002). Pairs between the central galaxy and satellite galaxies follow a separation function  $f_{\text{cs}}(r) = 4\pi\tilde{\rho}(r)r^2$ , with  $\tilde{\rho}(r)$  the normalized density distribution of the halo, which integrates to a total halo mass of unity. Satellite-satellite pairs follow a different separation function  $f_{\text{ss}}(r)$  which can also be obtained from the halo density distribution. The separation function for all pairs,  $f(r)$ , can be written as

$$\langle N_{\text{pair}}(M) \rangle f(r) \, dr = \langle N_{\text{cs}}(M) \rangle f_{\text{cs}}(r) \, dr + \langle N_{\text{ss}}(M) \rangle f_{\text{ss}}(r) \, dr \quad (33)$$

where  $\langle N_{\text{cs}}(M) \rangle$  and  $\langle N_{\text{ss}}(M) \rangle$  correspond to the average number of central-satellite and satellite-satellite pairs, respectively.

Once the CLF and  $\langle N_{\text{pair}}(M) \rangle f(r)$  are specified,  $\xi_{gg}(r)$  can be computed (see Appendix A). Figure 6 plots  $\xi_{gg}(r)$  for the late-type galaxies (dotted lines), the early-type galaxies (dashed lines) and the combined sample of galaxies (solid lines) for different luminosity bins and models. In addition, we plot the dark matter mass correlation function (dot-dashed lines) for comparison. Panels in the upper three rows show results for galaxies in magnitude intervals for which data from the 2dFGRS exists (Norberg et al. 2002). The panel in the lower row corresponds to  $-14 > M_{b_J} - 5\log h > -18$ . Since Norberg et al. only presented correlation functions for galaxies with  $M_{b_J} - 5\log h \leq -17.5$ , no data on  $\xi_{gg}(r)$  exists for this magnitude range.

Virtually all correlation functions, including that of the dark matter, reveal a special feature in the radial interval  $1h^{-1} \text{Mpc} \lesssim r \lesssim 3h^{-1} \text{Mpc}$ . This coincides with the transition from the 1-halo term to the 2-halo term (see Appendix A): at  $r \lesssim 1h^{-1} \text{Mpc}$  the correlation functions are governed by galaxy pairs within individual dark matter haloes and therefore depend on our assumptions regarding  $\langle N_{\text{pair}}(M) \rangle f(r)$ . For  $r \gtrsim 3h^{-1} \text{Mpc}$ , however, the galaxy correlation functions are independent of how galaxies are distributed inside haloes and only depend on the first moments  $\langle N(M) \rangle$  of the halo occupation number distributions.

Typically, at  $r \lesssim 2h^{-1} \text{Mpc}$  the ratio of the correlation functions of the early- and late-type galaxies is larger than at  $r \gtrsim 2h^{-1} \text{Mpc}$ . Since at small scales the clustering strength depends on the second moment of the occupancy numbers, the correlation function at small  $r$  is more dominated by the contribution from massive haloes than at large  $r$ . The ratio between the  $\xi_{gg}(r)$  of early- and late-type galaxies at small  $r$  is therefore sensitive to  $\mathcal{F}_l(M)$  at large  $M$ . This is immediately apparent from a comparison with the lower left panel of Figure 3, which shows that models A and C are

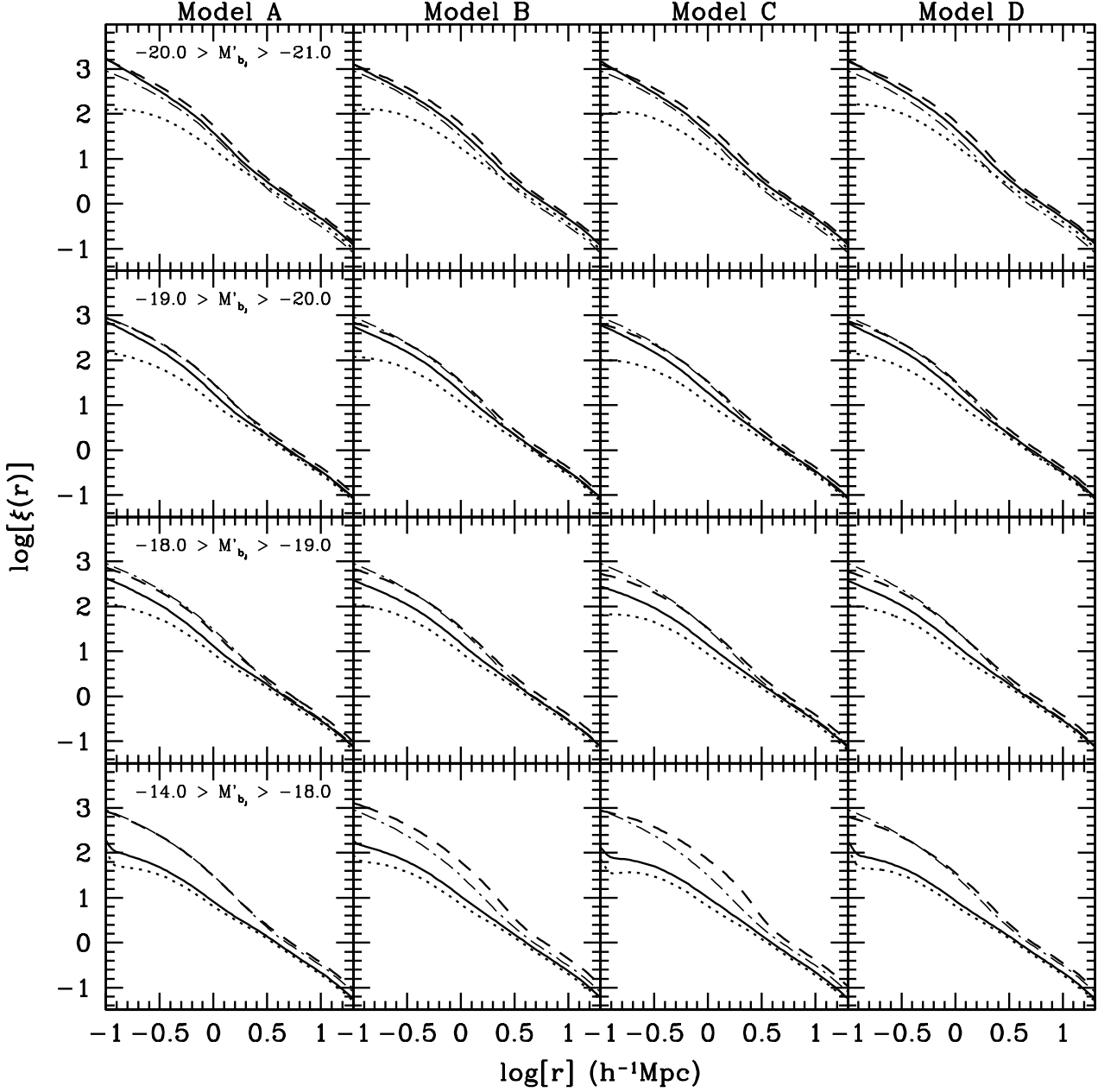


**Figure 6.** Real-space correlation functions of all galaxies (solid lines), late-type galaxies (dotted lines), and early-type galaxies (dashed lines). Results are shown for four different models, and for four different magnitude bins (as indicated). Note that  $M'_{b_J}$  is defined as  $M_{b_J} - 5\log h$ . The dot-dashed curves in each panel correspond to the real-space correlation function of the evolved, non-linear dark matter mass distribution, and is plotted for comparison. Note that the ratio between the correlation functions of early- and late-type galaxies increases with decreasing  $r$ . See text for a detailed discussion.

very similar with lower late-type fractions than models B and D. Consequently, the ratio of  $\xi_{gg}(r)$  of early- and late-type galaxies at small  $r$  is larger for models A and C than for models B and D.

As is also immediately apparent from Figure 6, the bias of galaxies with respect to the dark matter mass distribution depends sensitively on galaxy luminosity, on the radial scale, and on galaxy type (see also Kauffmann, Nusser & Steinmetz 1997). In general, early-type galaxies are biased tracers of the mass distribution at all scales, and for all luminosities, whereas late-type galaxies are virtually always anti-biased.

The combined sample of early- and late-type galaxies reveals a transition from positive bias at large scales ( $r \gtrsim 2h^{-1}\text{Mpc}$ ) to anti-bias at smaller scales, except for the most luminous galaxies which are always positively biased.

### 6.1 Comparison with observations

Can we compare these  $\xi_{gg}(r)$  to those obtained from the 2dFGRS? Norberg et al. (2002) argued that the real-space correlation functions of all subsamples of the 2dFGRS data are well fit by a single power-law (independent of luminos-

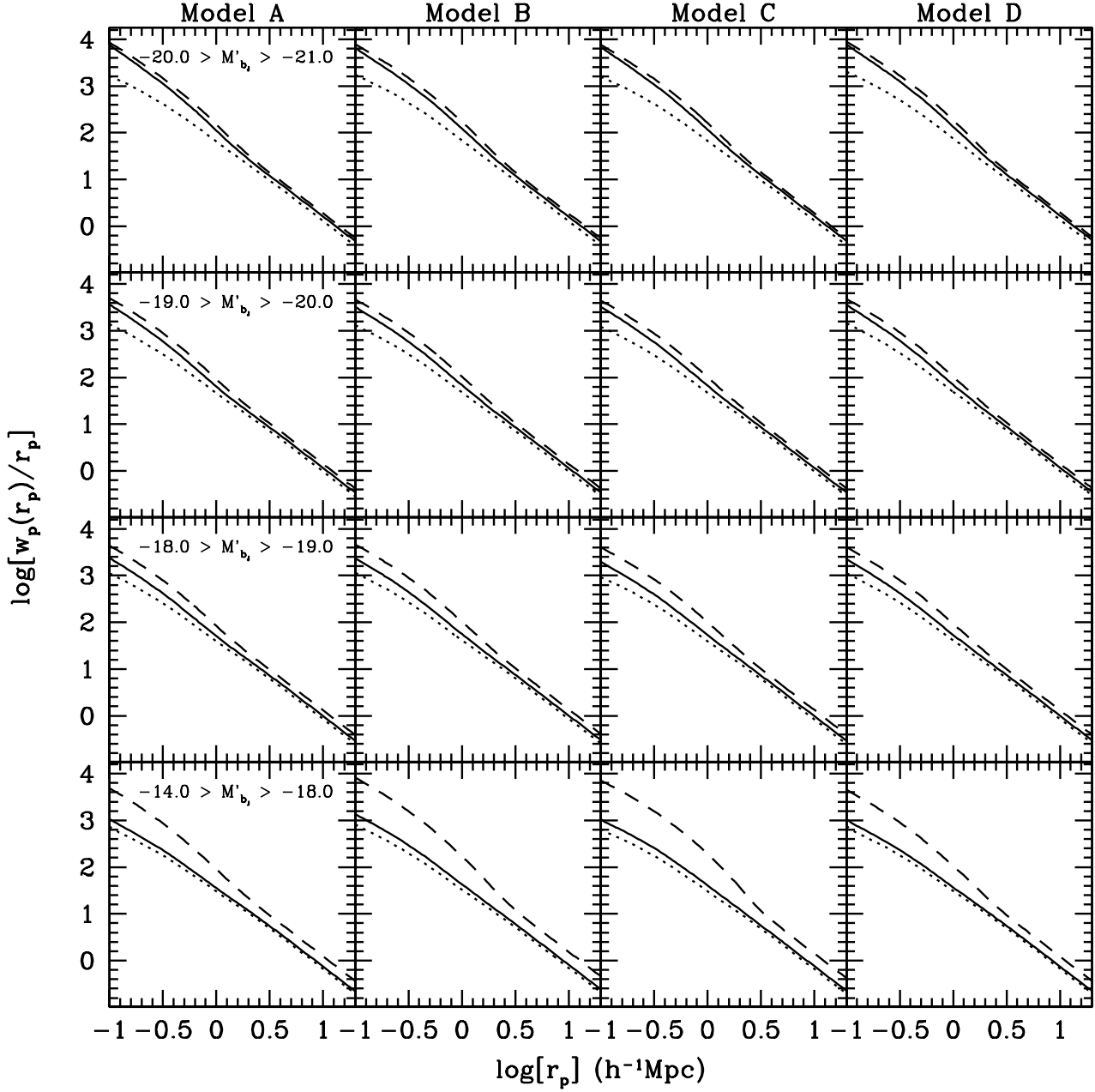


**Figure 7.** Same as Figure 6, except that here we plot the projected correlation function  $w_p(r_p)/r_p$  instead of the real-space correlation function  $\xi(r)$ . Note that these projected correlation functions, which unlike the real-space correlation functions can be directly obtained from redshift surveys, are much smoother than the real-space correlation functions and much better resemble single power-laws.

ity or spectral type). Taken at face value, the fact that virtually all correlation functions shown in Figure 6 reveal clear deviations from pure power-laws would force us to rule against each of our models. However, it is important to take into account how real-space correlation functions are obtained from data. After all, the data only yields a *redshift*-space correlation function, which is distorted with respect to the real-space correlation function due to the peculiar motions of the galaxies. On small scales the virialized motion of galaxies within dark matter haloes cause a reduction of the correlation power (the so-called ‘‘finger-of-God’’ effect), while on larger scales the correlations are boosted due to coherent flows (Kaiser 1987). It is common practice to

therefore compute the galaxy correlation function on a two-dimensional grid of pair separations parallel ( $\pi$ ) and perpendicular ( $r_p$ ) to the line-of-sight. Integration of this  $\xi_{gg}(r_p, \pi)$  over  $\pi$  then yields what is called the projected correlation function, which is related to the real-space correlation function by an Abel transform

$$w_p(r_p) = \int_{-\infty}^{\infty} \xi_{gg}(r_p, \pi) d\pi = 2 \int_{r_p}^{\infty} \xi_{gg}(r) \frac{r dr}{\sqrt{r^2 - r_p^2}} \quad (34)$$

(Davis & Peebles 1983). If the real-space correlation function is a single power-law,  $\xi_{gg}(r) = (r/r_0)^\gamma$  then the projected correlation function also follows a single power-law  $w_p(r_p)/r_p = A(\gamma)(r_p/r_0)^\gamma$  with

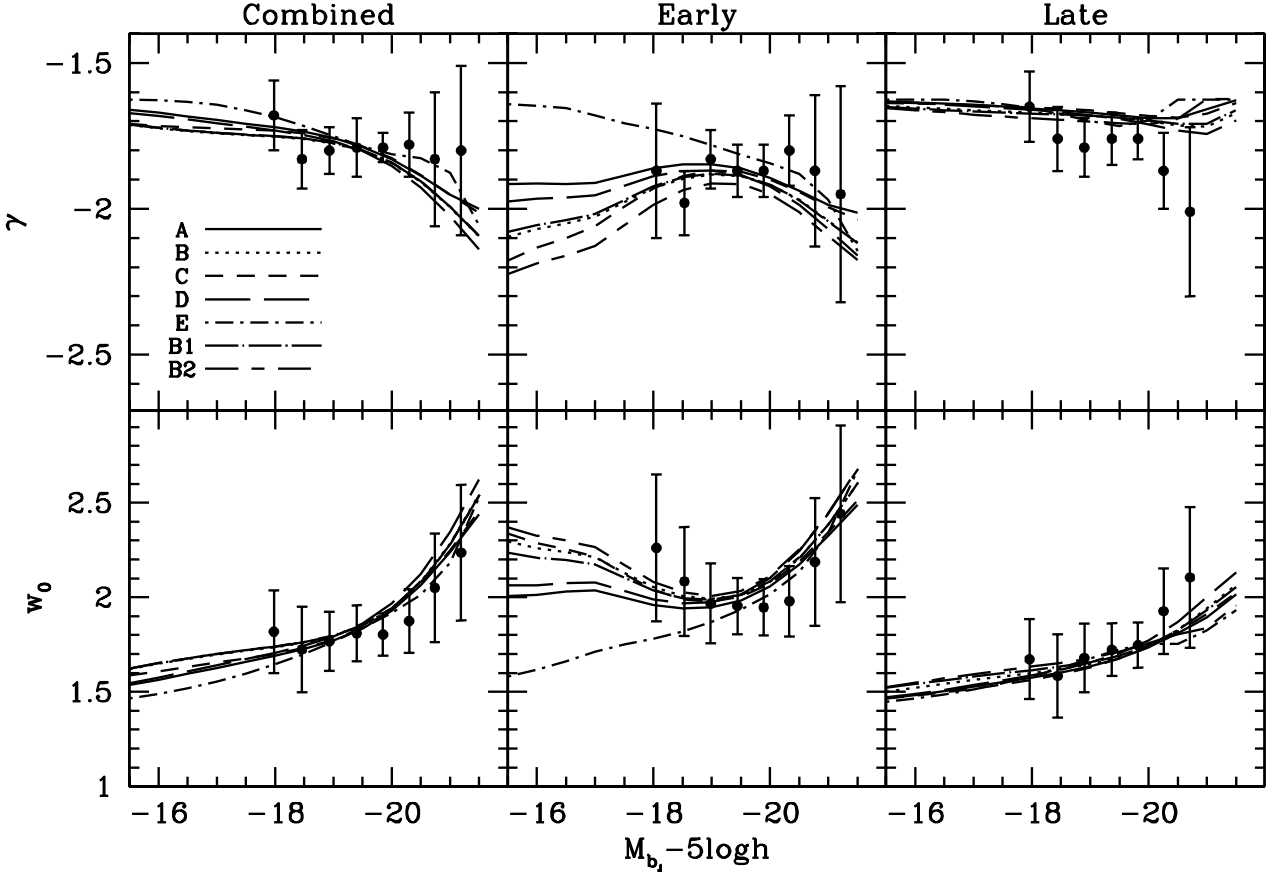


**Figure 8.** The power-law slopes  $\gamma$  and zero-points  $w_0$  of the projected correlation functions of galaxies within a one magnitude luminosity bin, obtained from a single power-law fit over the range  $-0.5 \leq \log(r_p) \leq 1.3$ . Symbols with errorbars correspond to the 2dFGRS data of Norberg et al. (2002), while the various lines indicate predictions from our models, as indicated. The overall agreement with the data is reasonable. Except for the relatively faint early-type galaxies, differences between the various models are small. Further constraints will have to await larger redshift surveys (i.e., smaller errorbars).

$$A(\gamma) = \frac{\Gamma(1/2) \Gamma(-(\gamma+1)/2)}{\Gamma(-\gamma/2)} \quad (35)$$

(see e.g., Baugh 1996).

In Figure 7 we plot  $w_p(r_p)/r_p$  (obtained using equation [34]) for the same samples of galaxies as in Figure 6. As can be seen, the projection has largely washed-out the features at  $\sim 2h^{-1}$  Mpc in the real-space correlation functions, and overall the projected correlation functions better resemble single power-laws. Only the correlation functions of early-type galaxies with  $-14 > M_{b,J} - 5\log h > -18$ , for which no data exists to date, clearly deviates from a single power-law.

In order to compare our models to the 2dFGRS data in a more quantitative way, we proceed as follows. For each spectral type and each luminosity bin Norberg et al. (2002) have fit a single power-law relation of the form  $w_p(r_p)/r_p = A(\gamma)(r_p/r_0)^\gamma$  to the projected correlation functions obtained from the 2dFGRS data. We rewrite this as

$$\log[w_p(r_p)/r_p] = w_0 + \gamma \log(r_p) \quad (36)$$

and compute  $w_0 = \log A(\gamma) - \gamma \log r_0$  and its error from the values of  $r_0$  and  $\gamma$  (and their errors) quoted by Norberg et al. (2002). The results are shown in Figure 8 (open circles with errorbars). Next, for each of our models we fit

equation (36) to the projected correlation functions over the same radial interval over which Norberg et al. (2002) fitted the data ( $-0.5 \leq \log(r_p) \leq 1.3$ ).

Our best-fit  $w_0$  and  $\gamma$  are shown in Figure 8 for all models listed in Table 1. Overall, the models fit the data reasonably well. Although the models predict somewhat more pronounced dependencies of  $\gamma$  and  $w_0$  on luminosity, and somewhat shallower correlation functions for the late-type galaxies, the errorbars on the data are too large to rule against any of these models. The level of agreement is actually quite surprising in light of the oversimplified assumptions regarding  $\langle N_{\text{pair}}(M) \rangle$  and  $f(r)$ . In particular, the assumption of sub-Poissonian occupation distributions may be a poor assumption on the scale of clusters (Benson et al. 2000; Scoccimarro et al. 2001, Cooray 2002). In addition, we have assumed that  $f(r)$  is independent of galaxy type and or luminosity (except for the brightest galaxy, which is always assumed to reside at the center). However, it is well known that clusters of galaxies reveal a radial morphology segregation (Abraham et al. 1996; van Dokkum et al. 1998; Balogh et al. 1999), with early-type (late-type) galaxies more confined towards the center (outer regions). Although morphological segregation within individual haloes is easy to take into account (e.g., Scranton 2002a,b), such a detailed investigation is be-

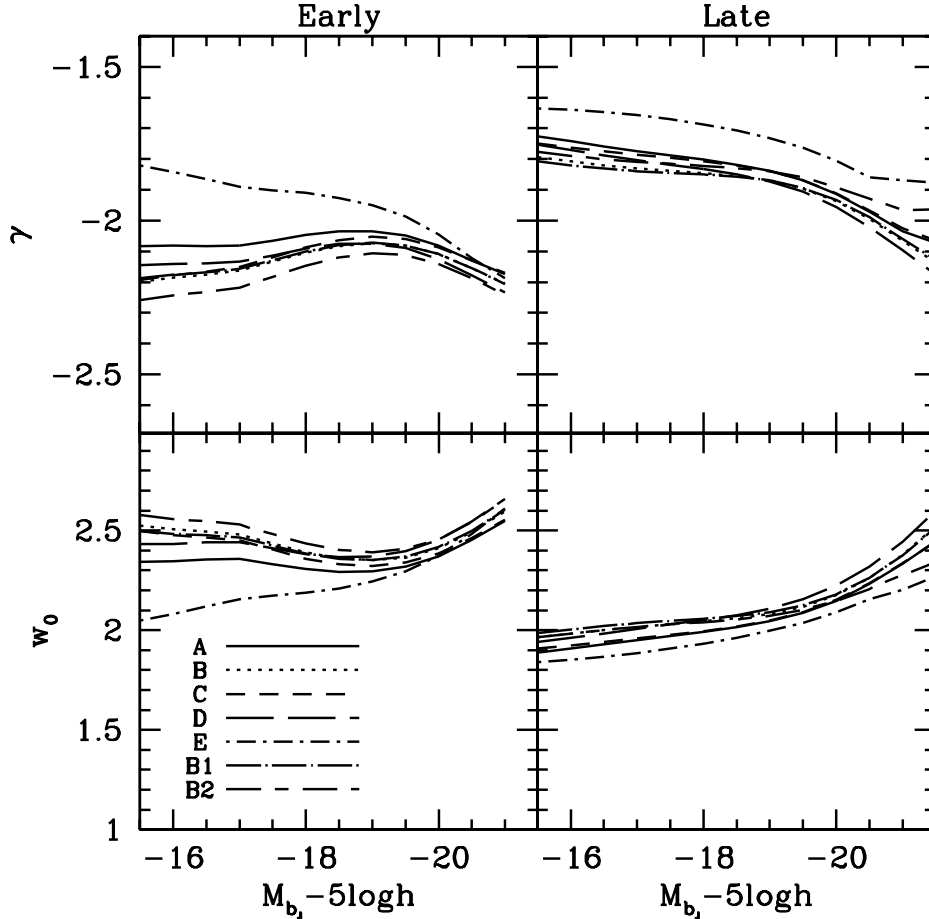


**Figure 9.** The power-law slopes  $\gamma$  and zero-points  $w_0$  of the projected cross-correlation functions with bright ( $-21 > M_{b_j} - 5\log h > -22$ ) early-type galaxies. As in Figure 8  $\gamma$  and  $w_0$  are obtained from a single power-law fit over the range  $-0.5 \leq \log(r_p) \leq 1.3$ .

yond the scope of this paper. However, we intend to return to this issue in a future paper.

Figure 8 also shows predictions for  $\gamma$  and  $w_0$  for galaxies down to  $M_{b_j} - 5\log h = -15.5$ . This shows that the main difference between the various models occurs for faint early-type galaxies. Furthermore, whereas the models predict very little luminosity dependence in the projected correlation function of late-type galaxies (except for a modest increase of the normalization with luminosity), for the early-type galaxies a very pronounced luminosity dependence is predicted. In particular, the models predict that early-type galaxies with  $M_{b_j} - 5\log h = -19.5$  (i.e., roughly  $L^*$ ), are less strongly clustered and with a shallower power-law slope than both brighter and fainter early-type galaxies (except for model E). Future data from the completed 2dFGRS and/or the SDSS will prove very useful in further testing and constraining the CLF models presented here.

In summary, once assumptions are made regarding the second moments of the halo occupation numbers and the spatial distribution of galaxies within individual dark matter haloes, the two-point correlation functions of galaxies *in any magnitude interval* can be computed from the CLFs. Because the fraction of late-type galaxies decreases with increasing halo mass, late-type galaxies are less strongly clustered than their early-type counterparts at small separa-

tions. This results in steeper projected correlation functions for the early-type galaxies, in qualitative agreement with the data. The remaining discrepancies, although small, are most likely a reflection of the fact that we have not taken the spatial segregation of morphological types in clusters into account. Finally we stress that accurate correlation functions of faint early-type galaxies are required in order to break the degeneracy present in the current models for the CLF.

## 6.2 Cross correlation functions

In addition to the (auto) correlation functions presented above, the CLFs also allow the computation of various cross correlation functions. As an example, Figure 9 plots the zero-point  $w_0$  and power-law slope  $\gamma$  of the projected cross-correlations with bright ( $-21 > M_{b_j} - 5\log h > -22$ ) early-type galaxies. Compared to the auto-correlation functions (Figure 8) the cross correlation functions are steeper and with a higher zero-point  $w_0$ . This is due to the fact that bright early-type galaxies reside predominantly in massive clusters. In addition, compared to the auto-correlation functions, the late-type galaxies reveal a more pronounced dependence of  $\gamma$  on luminosity. This is due to the fact that clusters are predominantly occupied by early-type galaxies: Faint late-type galaxies reside mainly in low-mass haloes,

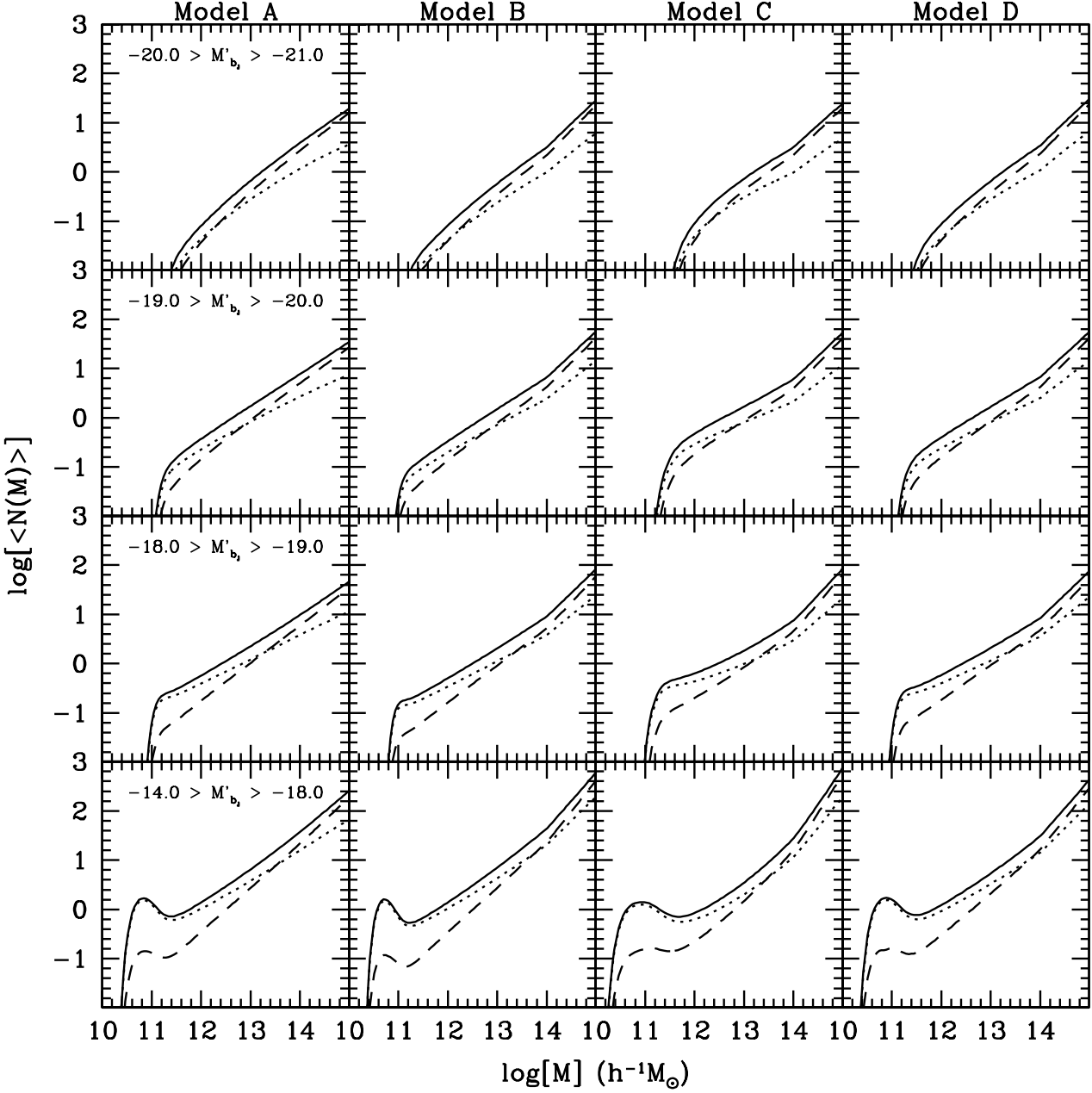


**Figure 10.** Halo occupation numbers for the same magnitude bins and models as in Figures 6 and 7. Dotted and dashed lines correspond to the late- and early-type galaxies, respectively. See text for a detailed discussion.

and are therefore relatively weakly correlated with bright early-type galaxies. The brightest late-type galaxies, on the other hand, are still predominantly found in massive clusters, and therefore strongly correlated with the bright early-types. Note that these predictions are likely to depend fairly strongly on the presence of a radial morphology segregation in clusters, which is not taken into account here. Therefore, Figure 9 should not be taken as a strong prediction, but merely serves to illustrate the power of the CLF method for computing various statistical properties of the galaxy distribution.

## 7 HALO OCCUPATION NUMBERS

We now use the CLFs to compute halo occupation numbers using equation (10). Results are shown in Figure 10 for the same samples of galaxies as in Figures 6 and 7. Although there are small differences amongst the four models presented here, several trends are shared by all models. First of all, one finds that the derivative  $d\langle N \rangle / dM$  is larger when brighter galaxies are considered. Secondly, when sufficiently faint galaxies are included,  $d\langle N \rangle / dM$  depends more strongly on mass (i.e.,  $\langle N(M) \rangle$  deviates more from a single power-law) in the sense that it decreases towards lower  $M$ . We can understand this behavior by focusing on the contributions of the late- and early-type galaxies. In all cases we find that

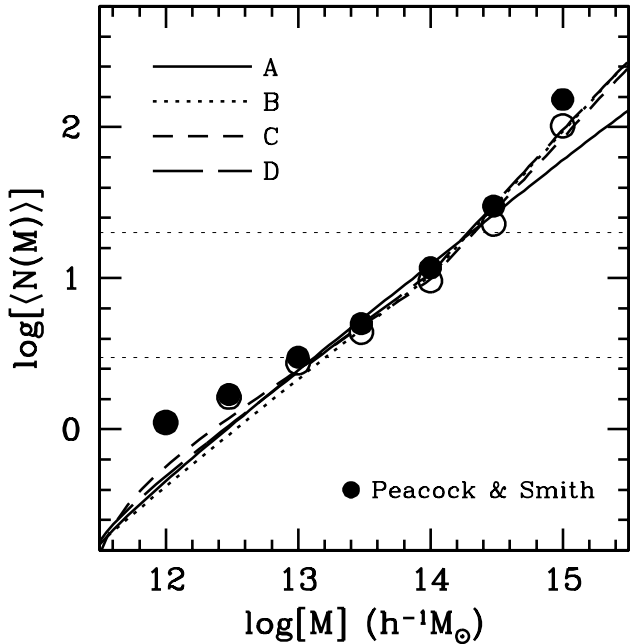


**Figure 11.** A comparison of the halo occupation numbers obtained by Peacock & Smith (2000, solid dots) and our CLFs for models A, B, C, and D (various lines). The open circles correspond to the halo occupation numbers obtained after replacing  $N$  with  $N^{0.92}$  as suggested by Peacock & Smith for haloes at the high mass end. The two dotted, horizontal lines indicate the range in  $N$  over which Peacock & Smith were able to constrain their models *directly* from data.

$d\langle N \rangle / dM$  is largest for the early-type galaxies. At large  $M$  and  $L$ , the majority of galaxies are early-types, and  $\langle N(M) \rangle$  is well fit by a single power-law. At lower  $L$  the fraction of late-type galaxies increases, predominantly at lower masses, such that a transition occurs from being dominated by late-type galaxies (at low  $M$ ) to being dominated by early-type galaxies (at high  $M$ ). Finally, note that  $\langle N(M) \rangle$  is always truncated at low  $M$ , indicating the presence of a minimum halo mass that can harbor a galaxy of a given luminosity. In terms of our models, this truncation is a reflection of  $\tilde{L}^*(M)$ .

### 7.1 Comparison with previous work

Several studies in the past have used a variety of methods to constrain  $\langle N(M) \rangle$  from observations. Jing, Mo & Börner (1998), using the two-point correlation function and pairwise velocity dispersions from the Las Campanas Redshift Survey (LCRS; Shectman et al. 1996), obtained  $N \propto M^{0.92}$ . Scoccimarro et al. (2001) fitted the measurements of counts-in-cells from the APM survey (Maddox et al. 1990) deprojected into three dimensions by Gaztañaga (1994), and found that  $N \propto M^{0.8}$  is required in the high mass limit.

Unfortunately, a direct comparison of these results with each other or with predictions from our CLFs is complicated for several reasons. First of all, the results obtained by Jing et al. (1998) and Scoccimarro et al. (2001) are based on *apparent magnitude* limited samples, which are difficult to compare to halo occupation numbers in absolute magnitude ranges, such as those obtained from the CLFs. Secondly, the LCRS is based on *R*-band data for which halo-occupation

numbers are not expected to be the same as in the *b\_J*-band used here and by Scoccimarro et al. In fact, as shown by Jing et al. the two-point correlation function of the LCRS is significantly steeper than that of the APM survey on which the 2dFGRS data is based.

Peacock & Smith (2000; hereafter PS00), on the other hand, presented halo occupation numbers for galaxies with  $M_{b_J} \leq -19.0$ , which we can compare directly to predictions from our CLFs. Using data on galaxy groups from the CfA survey (Ramella, Pisani & Geller 1997) and the ESO Slice Project (Ramella et al. 1999), PS00 found that the number density of groups containing  $N$  galaxies obeys  $\rho(N) \propto N^{-2.7}$ . Equating the number density of groups with multiplicity larger than  $N$  to the number density of dark matter haloes with mass larger than  $M$ , results in the halo occupation numbers shown by solid dots in Figure 11. For comparison, we also show the predictions for our CLF models A, B, C, and D (various lines). Over the intermediate mass range  $2 \times 10^{13} h^{-1} M_\odot \lesssim M \lesssim 5 \times 10^{14} h^{-1} M_\odot$  the PS00 estimates agree well with the occupation numbers obtained here. However, at both lower and higher masses the  $\langle N(M) \rangle$  of PS00 are significantly higher than in any of our four models. The data used by PS00 was restricted to groups with  $3 \leq N \leq 20$  (indicated by dotted, horizontal lines). For  $N > 20$  PS00 simply extrapolated the power-law behavior of  $\rho(N)$  to higher multiplicity. As PS00 argued themselves, these results may not be completely reliable, and PS00 therefore suggested to replace  $N$  with  $N^{0.92}$  at the high mass end. This is indicated by the open circles in Figure 11 and brings the PS00 results in good agreement with the  $\langle N(M) \rangle$  of our models B, C, and D for haloes with  $M \gtrsim 2 \times 10^{13} h^{-1} M_\odot$ . For  $N < 3$  the disagreement remains. However, here PS00 extrapolated the power-law behavior of  $\rho(N)$  down to  $N = 2$  and obtained the result for  $N = 1$  by matching the number density of galaxies to the observed value. Given the uncertainties involved, it is encouraging that these two results, based on completely different methods, agree as well as they do.

## 8 COMPARISON WITH SEMI-ANALYTICAL MODELS

In this paper we have derived conditional luminosity functions for late- and early-type galaxies. We have shown that although some degeneracy remains, the overall behavior of  $\langle M/L \rangle$  and  $\langle N(M) \rangle$  is well constrained. We thus have obtained important constraints on how galaxies have to be distributed over dark matter haloes in order to yield luminosity functions and correlation lengths in agreement with the data. The important question that arises is whether such halo occupancy distributions can be obtained within the standard framework for galaxy formation; i.e., how do the cooling, feedback and star formation efficiencies depend on halo mass, such that one can reproduce the CLFs obtained here.

In order to address this question we compare our results with several semi-analytical (SA) models in the literature. These SA models use various phenomenological prescriptions to describe the star formation, feedback, and cooling efficiencies which are linked to merger histories of dark matter haloes obtained from either the extended Press-Schechter

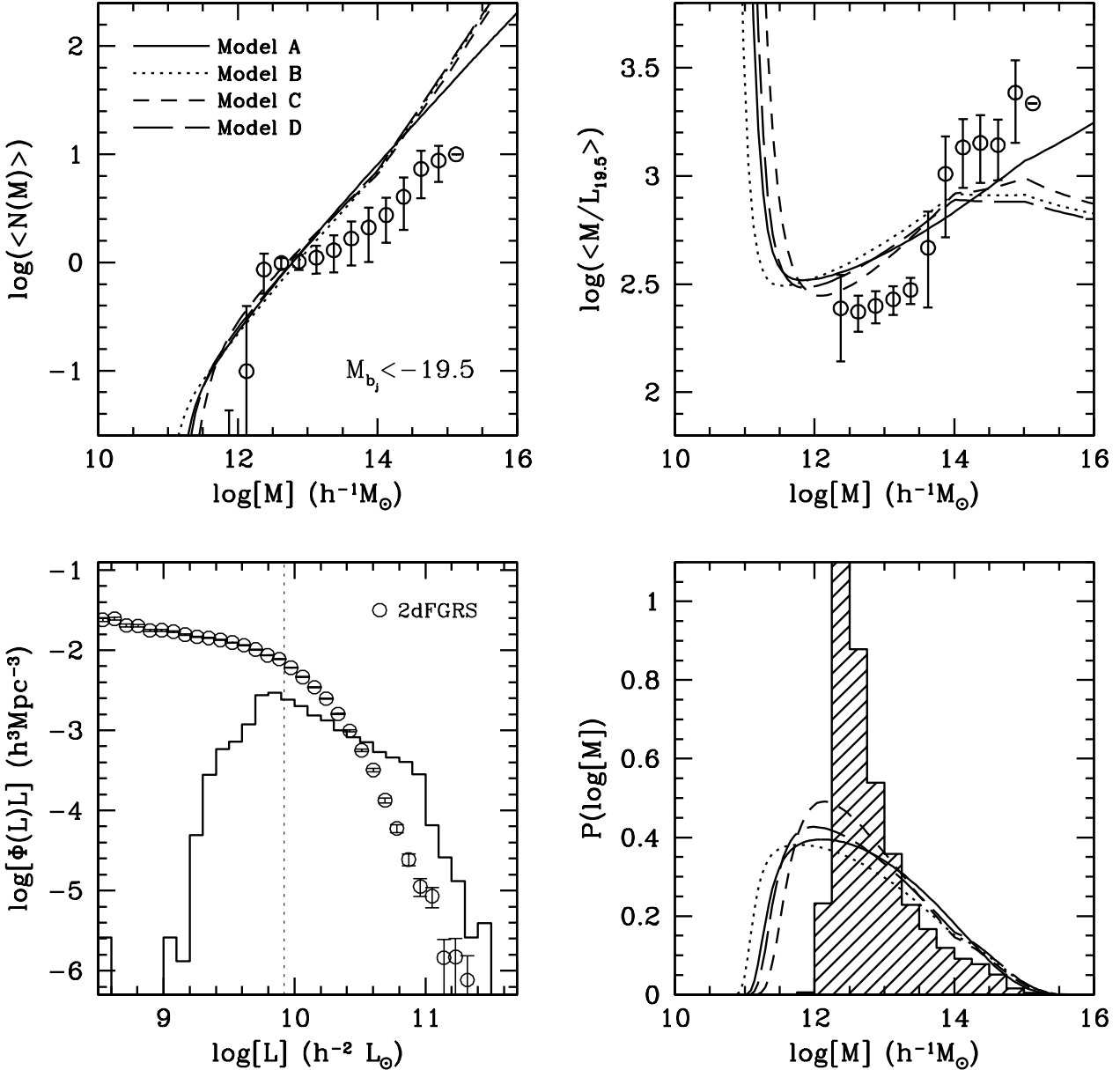


**Figure 12.** Comparison of the semi-analytical models of Kauffmann et al. (1999; K99) with models A, B, C, and D. Upper left panel plots the halo occupation numbers for galaxies with  $M_{b_J} - 5\log h < -19.5$ . Symbols correspond to the semi-analytical models, and lines to the CLF models, as indicated. Compared to our models, the SA-model underpredicts the average number of galaxies in massive haloes. The upper right panel plots the corresponding ratio of halo mass to the total luminosity  $L_{19.5}$  contributed by galaxies brighter than  $M_{b_J} - 5\log h = -19.5$ . The K99 model predicts higher (lower) values of  $M/L_{19.5}$  compared to the CLFs presented here at the high (low) mass end. The lower right panel plots the mass distribution of haloes hosting galaxies with  $M_{b_J} - 5\log h < -19.5$ . Again, the agreement between the K99 model and our CLF models is poor, with the latter predicting much broader halo mass distributions. The reason for these various discrepancies is that unlike for the CLF models presented here, the LF of the K99 model is strongly inconsistent with the observed LF. This is indicated in the lower left panel where symbols correspond to the 2dFGRS LF of Madgwick et al. (2002) while the histogram corresponds to the LF of the model galaxies of K99. The vertical dotted line indicates  $M_{b_J} - 5\log h = -19.5$ .

formalism (e.g., Lacey & Cole 1993), or directly from numerical simulations. Combined with stellar population models and recipes for the merging of galaxies within merging dark matter haloes these models yield, amongst others, luminosities of galaxies in haloes of different masses.

Here we compare our models with the SA models of Kauffmann et al. (1999; hereafter K99), Mathis et al. (2002;

hereafter M02), and Benson et al. (2002; B02)<sup>†</sup>. Each of these three models used exactly the same cosmological pa-

<sup>†</sup> The models of K99 and M02 are publicly available at <http://www.MPA-Garching.MPG.DE/~virgo/virgo/index-galaxy.html> while the model of B02 was kindly provided to us by Andrew Benson.

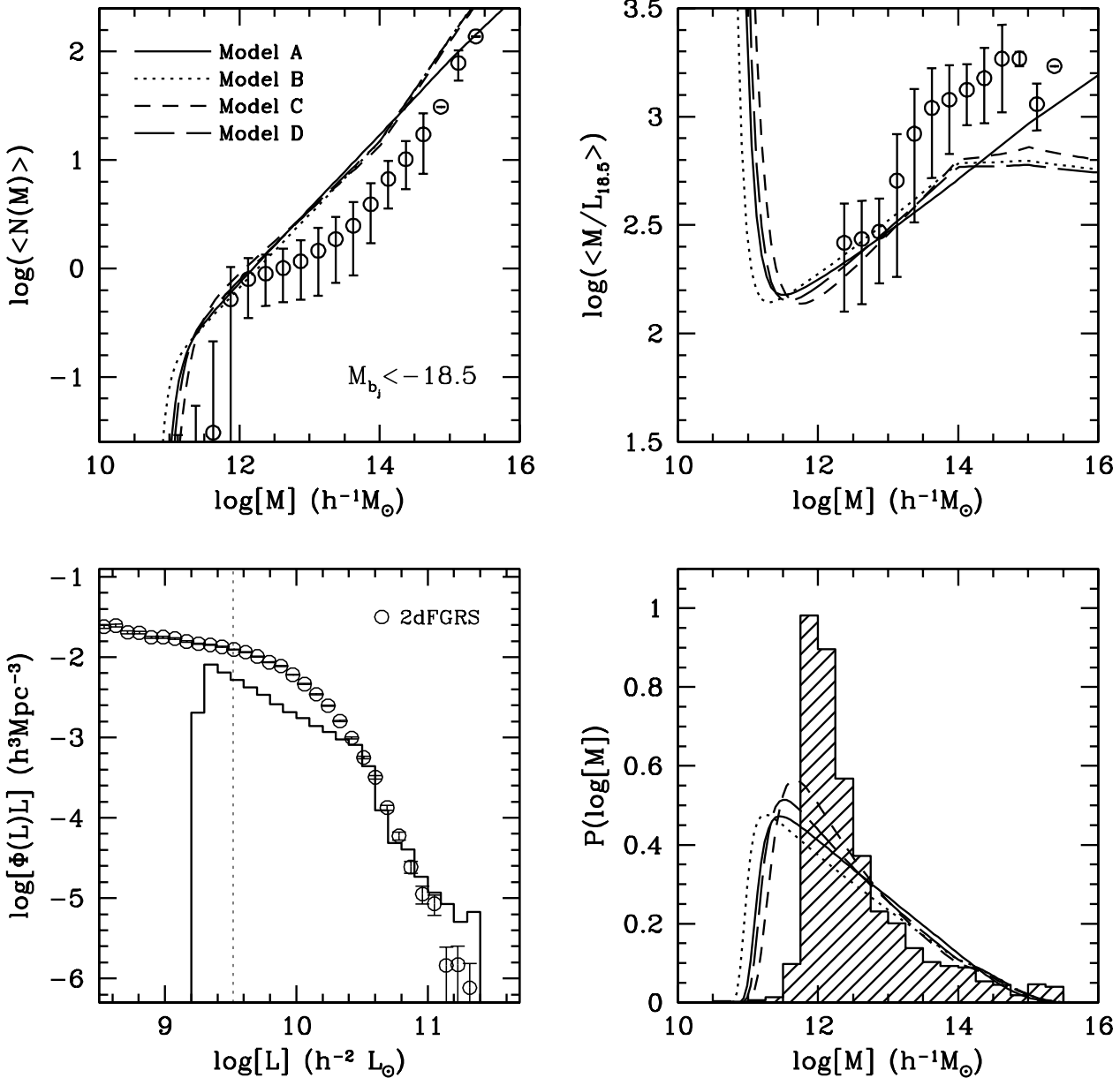


**Figure 13.** Same as Figure 12, except that here we compare our models to the SA model of Mathis et al. (2002; M02) for galaxies with  $M_{b_J} - 5\log h < -18.5$ . Since the LF of this SA model is in somewhat better agreement with the observations (see lower left panel), the overall agreement with our CLF models has also improved, though only marginally.

rameters as adopted here. K99 and M02 used numerical simulations to compute the merger histories of the dark matter haloes, and their models are consequently limited in halo mass by numerical resolution. The model of B02, on the other hand, is based on merger histories obtained using the extended Press-Schechter formalism (for details see Cole et al. 2000), and therefore allows a comparison with our models over a much larger range of halo masses and luminosities. The results of K99 and M02 are based on the same semi-analytical model, although the parameters used are somewhat different. Luminosities in the K99 model have not been corrected for dust extinction, whereas those in M02 have (though we have verified that this has only a very small effect on the results presented below). Both K99 and M02

tuned their model parameters to fit primarily the zero-point of the Tully-Fisher (TF) relation. This results in rather poor fits to the observed LF (see below). The model of B02 is significantly different. It is based on the semi-analytical models of Cole et al. (2000) but with (i) an improved prescription for the effects of tidal stripping and dynamical friction, and (ii) a model for feedback from the photoionizing background. Unlike in K99 and M02, B02 tune their parameters to reproduce the 2dFGRS LF of Madgwick et al. (2002), which results in a TF zero-point that is offset from the observed value (see discussion below).

Before we can make a fair comparison we need to adopt a consistent definition of halo masses. Both the SA models of K99 and M02 provide two measures for the halo mass

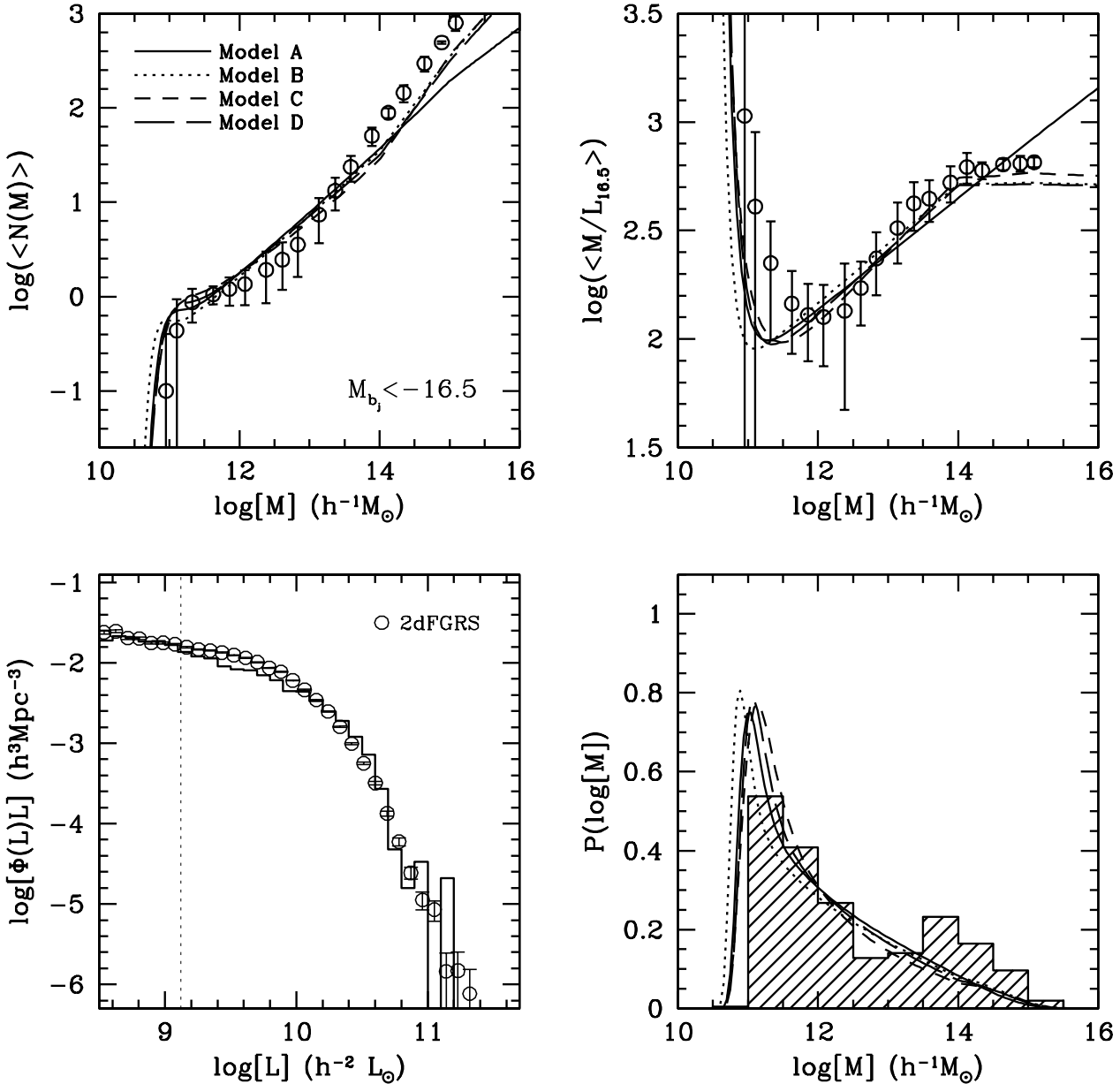


**Figure 14.** Same as in Figures 12 and 13 but for the semi-analytical model of Benson et al. (2002; B02) for galaxies with  $M_{b_J} - 5\log h < -16.5$ . Contrary to those of K99 and M02, this model agrees well with both our CLF models and with the observed 2dFGRS LF. Since B02 tuned their model parameters to reproduce this particular LF, the latter does not come as a surprise. However, the good agreement for the halo occupation numbers, mass-to-light ratios, and halo mass distributions with our CLF models is remarkable given the completely different nature of both techniques. The remaining disparities between the SA model and our CLF models can be contributed to the remaining disagreement between the observed LF and that of the B02 model.

associated with each galaxy;  $M_{\text{FOF}}$ , the mass of the halo obtained using the standard friends-of-friends (FOF) algorithm (Davis et al. 1985) with a linking length of  $b = 0.2$  times the mean inter-particle separation, and  $M_{200}$ , the mass of a sphere centered on the most-bound-particle of the FOF group with a radius inside of which the average density is 200 times the *critical* density. For each individual halo  $M_{\text{FOF}}$  and  $M_{200}$  can differ substantially, and therefore the results are sensitive to which halo mass we adopt. Since our models rely on the Sheth & Tormen (1999) halo mass function, and since Jenkins et al. (2001) have shown that this is in

very good agreement with the mass function of FOF groups with a linking length of  $b = 0.2$ , we use  $M_{\text{FOF}}$ . B02 define their halos as spheres with an average overdensity of 320. We convert these masses to  $M_{180}$ , consistent with the definition of halo mass used throughout this paper, assuming that dark matter halos follow the NFW density distribution (Navarro, Frenk & White 1992) with a concentration parameter given by Eke, Navarro & Steinmetz (2001). Next we need to be careful about the use of luminosities. The SA models give for each galaxy the absolute magnitudes in the  $B$  and  $V$  bands. In order to allow a fair comparison with

our models, we compute for each galaxy  $M_{b_J} - 5\log h$  using  $b_J = B - 0.28(B - V)$  (Blair & Gilmore 1982) and adopting the Hubble constant used in the models ( $h = 0.7$ ).

We first compare our results with the model of K99. Because of the numerical resolution of the simulation used by K99, only galaxies with a stellar mass  $M_* \geq 1.4 \times 10^{10} h^{-1} M_\odot$  are available. Although this includes galaxies down to  $M_{b_J} - 5\log h \simeq -18$ , the sample of model galaxies is only complete down to  $M_{b_J} - 5\log h = -19.5$ . When comparing for instance halo occupation numbers, completeness is important and we therefore limit ourselves here to a comparison of galaxies with  $M_{b_J} - 5\log h \leq -19.5$ . The upper left panel of Figure 12 plots the number of galaxies with  $M_{b_J} - 5\log h \leq -19.5$  as function of halo mass. Open circles correspond to the K99 model, with errorbars indicating the rms scatter. In addition, we show the predictions for models A, B, C, and D (various lines). Differences between these four models are typically small. For  $M > 10^{13} h^{-1} M_\odot$  the SA model predicts fewer galaxies per halo than our CLF models, while the opposite is true for haloes with  $M \sim 5 \times 10^{12} h^{-1} M_\odot$ . The upper panel on the right plots  $\langle M/L_{19.5} \rangle$  as function of halo mass. Here  $L_{19.5}$  is defined as the total luminosity of galaxies with  $M_{b_J} - 5\log h \leq -19.5$  in each individual halo. For  $M > 10^{14} h^{-1} M_\odot$  the SA model overpredicts  $\langle M/L_{19.5} \rangle$  compared to our CLF models, in agreement with the fact that K99 predicts lower occupation numbers. However, at  $M \simeq 10^{13} h^{-1} M_\odot$ , where both the SA and CLF models predict on average one galaxy per halo, the former predicts significantly lower  $\langle M/L_{19.5} \rangle$ . This indicates that the average luminosity of galaxies in haloes with  $M = 10^{13} h^{-1} M_\odot$  is higher in the SA model than in our CLF models. Finally, the lower right panel plots the mass distribution of haloes harboring galaxies with  $M_{b_J} - 5\log h \leq -19.5$ . Note that a halo containing  $N$  such galaxies is counted  $N$  times. The hatched histogram corresponds to the SA model, whereas the various lines show predictions for our CLF models computed from

$$P(M) dM = \frac{\int_{L_{\min}}^{\infty} \Phi(L|M) dL}{\int_{L_{\min}}^{\infty} \Phi(L) dL} n(M) dM. \quad (37)$$

with  $L_{\min}$  the lower luminosity limit of the sample. Again the agreement between the SA and CLF models is extremely poor, with the latter predicting much broader mass distribution functions. None of these disagreements, however, come as a surprise. After all, as shown in the lower left panel, the K99 model predicts a LF that is in very poor agreement with the observed LF of the 2dFGRS, and thus also with the LFs corresponding to our CLF models.

Figure 13 shows a similar comparison but now with the SA model of M02. Since the numerical simulations used by M02 have somewhat higher numerical resolution, we can extend our comparison down to  $M_{b_J} - 5\log h = -18.5$ . Mathis et al. (2002) focussed on modeling the *local* galaxy population, using numerical simulations constrained to reproduce the local smoothed linear density field out to a distance of  $8000 \text{ km s}^{-1}$ . Since this corresponds to a cosmological volume that is smaller than that in K99, the errorbars are somewhat larger. As shown in the lower left panel, the M02 model significantly improves the agreement with the observed LF at the bright-end compared to K99, even though it still severely underpredicts the number of galaxies

with  $M_{b_J} - 5\log h \gtrsim -20$ . This explains why the SA model predicts (i) smaller occupation numbers, (ii) higher mass-to-light ratios, and (iii) a higher mean halo mass for galaxies with  $M_{b_J} - 5\log h \leq -18.5$  compared to our CLF models.

Finally, in Figure 14 we compare our models to the SA model of B02. Since numerical resolution does not play a role here, we extend the comparison down to galaxies with  $M_{b_J} - 5\log h = -16.5$ . As shown in the lower left panel, the B02 model yields a much better fit to the observed LF than either the K99 or M02 models. Since B02 chose to tune their model parameters to fit this particular LF, rather than the zero-point of the TF relation, this does not come as a surprise. The good agreement with our CLF models, however, is not a trivial result. Although some amount of disagreement remains, this can all be attributed to the fact that the B02 model slightly over(under)-predicts the LF at luminosities just above (below)  $L^*$ . All in all, the agreement is extremely encouraging and seems to suggest that our CLFs correspond to a galaxy formation scenario that is very similar to the SA model of B02.

In summary, our CLF models imply halo occupation numbers and mass-to-light ratios that are in poor agreement with the semi-analytical models of K99 and M02, but in surprisingly good agreement with the model of B02. However, this does not mean that the B02 models are better or more reliable than the models of K99 and M02. Rather, the differences between the various SA models reflect a well known problem in galaxy formation theory, namely the inability of models to simultaneously fit the observed LF and zero-point of the TF relation (e.g., Kauffmann et al. 1993; Cole et al. 1994, 2000; Somerville & Primack 1999; Benson et al. 2000). In fact, this does not seem a problem related to the particular prescriptions for star formation and/or feedback used in these models, but to reflect a more fundamental problem related to the particular cosmological model: as we have shown in detail in Paper 1, even the CLF models, which are independent of how galaxies form, are inconsistent with the TF zero-point. Since both the SA model of B02 and our CLF models are tuned to fit the LF, one should not expect good agreement regarding halo occupation numbers with the K99 and M02 models, which are tuned to fit the TF zero-point. However, it is extremely encouraging that the SA model that *does* fit the observed LF agrees remarkably well with our CLF models. The fact that these two wildly different techniques imply consistent mass-to-light ratios and halo occupation numbers, is an important step forward in our quest for a coherent picture of galaxy formation within a CDM cosmology. The question whether the occupation distributions inferred from our CLFs can be made consistent with the standard framework for galaxy formation thus seems to have a positive answer.

## 9 CONCLUSIONS

Data from large ongoing redshift surveys such as the SDSS and 2dFGRS provide a wealth of information on the clustering properties of galaxies as function of morphological type, luminosity, surface brightness, star formation rate, etc. At the same time, numerical simulations and sophisticated analytical techniques are continuously improving our understanding of the clustering properties of dark matter haloes

within CDM cosmologies. The ultimate challenge is to constrain how galaxies with different properties occupy haloes of different masses. This information not only gives an easy to interpret description of the galaxy-dark matter connection, but also yields important constraints on galaxy formation theories.

In this paper we have used recent observations from the 2dFGRS to constrain the CLFs of early- and late-type galaxies. Although some amount of degeneracy remains, the CLFs are well constrained. They indicate that the average mass-to-light ratios of dark matter haloes have a minimum of  $\sim 100h(M/L)_\odot$  around a halo mass of  $\sim 3 \times 10^{11}h^{-1}M_\odot$ . Towards lower masses  $\langle M/L \rangle$  increases rapidly, and matching the faint-end slope of the observed LF requires that haloes with  $M < 10^{10}h^{-1}M_\odot$  are virtually devoid of galaxies producing light. At the high mass end, the observed clustering properties of galaxies require that clusters have mass-to-light ratios (in the photometric  $b_J$  band) in the range of roughly  $500h(M/L)_\odot$  to  $1000h(M/L)_\odot$ . Finally, the fact that early-type galaxies are more strongly clustered than late-type galaxies requires that the fraction of late-type galaxies is a strongly declining function of halo mass, although the exact relation is currently poorly constrained. Forthcoming data from both the SDSS and the 2dFGRS will reduce the errors on the current measurements and provide correlation lengths down to fainter magnitudes, both of which are essential to further constrain the CLFs.

The halo occupation numbers  $\langle N(M) \rangle$  implied by these CLFs depend rather strongly on the magnitude interval of galaxies considered. Typically, including fainter galaxies results in weaker mass dependencies and a stronger departure from a single power-law form. This is mainly a reflection of the way in which early- and late-type galaxies contribute: early-type galaxies reveal a steeper  $\langle N(M) \rangle$  than the late-type galaxies. When only bright galaxies are considered,  $\langle N(M) \rangle$  is well fit by a single power-law (with a low mass cut-off) and is dominated by early-type galaxies. When sufficiently faint galaxies are included, the late-type galaxies start to dominate at the low mass end. Since these reveal a shallower  $\langle N(M) \rangle$  than early-type galaxies, the shape of  $\langle N(M) \rangle$  becomes more complicated. We have compared our halo occupation numbers with those obtained by Peacock & Smith (2000) from the multiplicity of galaxy groups. Except for haloes with  $\langle N \rangle \lesssim 3$ , where the results of Peacock & Smith are uncertain due to unreliable extrapolation, the agreement is remarkably good.

Once assumptions are made about the second moment of the halo occupation number distributions and the spatial distribution of galaxies within individual haloes, the two-point galaxy-galaxy correlation function can be computed from the CLFs presented here for any magnitude bin and for both early- and late-type galaxies (as well as their cross correlation). We presented a number of correlation functions under the assumptions that (i)  $P(N|M)$  is sub-Poissonian, (ii) the brightest galaxy always resides at the halo center, and (iii) the remaining satellite galaxies follow the density distribution of the dark matter. In order to facilitate a comparison with real data we also computed the projected correlation functions. For late-type galaxies, we find that the power-law slopes of these projected correlation functions are virtually independent of luminosity. For early-type galaxies, on the other hand, a fairly strong luminosity dependence is

predicted; early-type galaxies with luminosities around  $L^*$  are less strongly clustered, and with a shallower power-law slope, than early type galaxies with either  $L > L^*$  or  $L < L^*$ . A direct comparison with the slopes and zero-points of the projected correlation functions obtained from the 2dFGRS reveals good agreement. We also presented predictions for the cross correlation functions with bright early-type galaxies. Typically, these are stronger and steeper than the corresponding auto-correlation functions, which is a direct consequence of the fact that bright early-types reside predominantly in massive clusters.

Finally we have compared halo occupation numbers and mass-to-light ratios inferred from our CLFs with predictions from three different semi-analytical models for galaxy formation. Overall, the agreement between our models and the SA models of both K99 and M02 is extremely poor. However, the reason for this discrepancy is well understood. Both K99 and M02 have normalized their models to fit the zero-point of the TF relation. It is well known, that current models for galaxy formation fail to simultaneously fit the TF zero-point and the observed LF of galaxies. In fact, exactly the same problem was identified in Paper 1 based on modeling the CLF. Indeed, the models of K99 and M02 yield LFs that differ strongly from that of the 2dFGRS, and thus from those of our CLF models. It should not come as a surprise that therefore the halo occupation numbers and mass-to-light ratios do not match. Benson et al. (2002), however, presented a SA model that was normalized to fit the observed 2dFGRS LF. The agreement of this particular SA model with our CLF models is remarkably good. Given the completely different nature of both techniques to predict halo occupation numbers and mass-to-light ratios, this agreement is far from trivial. In fact, it indicates that the technique used here has recovered a statistical description of how galaxies populate dark matter haloes which is not only in perfect agreement with the data, but which in addition fits nicely within the standard framework for galaxy formation.

## ACKNOWLEDGEMENTS

We are grateful to Andrew Benson, Guinevere Kauffmann and Hugues Mathis for making the results from their semi-analytical models available, and to Robert Smith, John Peacock and Carlos Frenk for valuable discussion. XY thanks the MPG-CAS student exchange program for financial support, and FvdB thanks the Institute for Advanced Study in Princeton and the Department of Physics at New York University for their hospitality during visits in October 2002.

## REFERENCES

- Abraham R.G. et al., 1996, ApJ, 471, 694
- Bahcall N.A., Lubin L., Dorman V., 1995, ApJ, 447, L81
- Bahcall N.A., Cen R., Davé R., Ostriker J.P., Yu Q., 2000, ApJ, 541, 1
- Balogh M.L., Morris S.L., Yee H.K., Carlberg R.G., Ellingson E., 1999, ApJ, 527, 54
- Baugh, C.M., 1996, MNRAS, 282, 1413
- Beijersbergen M., Hoekstra H., van Dokkum P.G., van der Hulst T., 2002, MNRAS, 329, 385

Benson A.J., Cole S., Frenk C.S., Baugh C.M., Lacey C.G., 2000, MNRAS, 311, 793

Benson A.J., Lacey C.G., Baugh C.M., Cole S., Frenk C.S., 2002, MNRAS, 333, 156

Berlind A.A., Weinberg D.H., 2002, ApJ, 575, 587

Blair M., Gilmore G., 1982, PASP, 94, 741

Bullock J.S., Kolatt T.S., Sigad Y., Somerville R.S., Kravtsov A.V., Klypin A.A., Primack J.R., Dekel A., 2001, MNRAS, 321, 559

Bullock J.S., Wechsler, R.H., Somerville R.S., 2002, MNRAS, 329, 246

Cole S., Aragon-Salamanca A., Frenk C.S., Navarro J.F., Zepf S.E., 1994, MNRAS, 271, 781

Cole S., Lacey C.G., Baugh C.M., Frenk C.S., 2000, MNRAS, 319, 168

Colless M., et al., 2001, MNRAS, 328, 1039

Cooray A., 2002, ApJ, 576, L105

Cooray A., Sheth R., 2002, preprint (astro-ph/0206508)

Davis, M., Peebles, P.J.E., 1983, ApJ, 267, 465

Davis, M., Efstathiou G., Frenk C.S., White S.D.M., 1985, ApJ, 292, 391

Efstathiou G., Ellis R.S., Peterson B.S., 1988, MNRAS, 232, 431

Efstathiou G., Bond J.R., White S.D.M., 1992, MNRAS, 285, 1

Eke V.R., Navarro J.F., Steinmetz M., 2001, ApJ, 554, 114

Fardal M.A., Katz N., Gardner J.P., Hernquist L., Weinberg D.H., Dav'e R., 2001, ApJ, 562, 605

Fry J.N., 1996, ApJ, 461, L65

Fukugita M., Hogan C.J., Peebles P.J.E., 1998, ApJ, 503, 518

Gaztañaga E., 1994, MNRAS, 268, 913

Jenkins A., Frenk C.S., White S.D.M., Colberg J.M., Cole S., Evrard A.E., Couchman H.M.P., Yoshida N., 2001, MNRAS, 321, 372

Jing Y.P., 1998, ApJ, 503L, 9

Jing Y.P., Mo H.J., Börner G., 1998, ApJ, 494, 1

Jing Y.P., Börner G., Suto Y., 2002, ApJ, 564, 15

Kaiser N., 1987, MNRAS, 227, 1

Kang X., Jing Y.P., Mo H.J., Börner G., 2002, MNRAS, 336, 892

Katz N., Weinberg D.H., Hernquist L., 1996, ApJS, 105, 19

Kauffmann G., Nusser A., Steinmetz M., 1997, MNRAS, 286, 795

Kauffmann G., White S.D.M., Guiderdoni B., 1993, MNRAS, 264, 201

Kauffmann G., Colberg J.M., Diaferio A., White S.D.M., 1999, MNRAS, 303, 188

Kay S.T., Pearce F.R., Frenk C.S., Jenkins A., 2002, MNRAS, 330, 113

Kochanek C.S., White M., Huchra J., Macri L., Jarrett T.H., Schneider S.E., Mader J., 2002, preprint (astro-ph/0208168)

Lacey C., Cole S., 1993, MNRAS, 262, 627

Loveday J., Efstathiou G., Peterson B.A., Maddox S.J., 1992, ApJ, 400, L43

Ma C.P., Fry J.N., 2000, ApJ, 543, 503

Maddox S.J., Efstathiou G., Sutherland W.J., Loveday L., 1990, MNRAS, 242, 43

Madgwick D.S., 2002, preprint (astro-ph/0209051)

Madgwick D.S., et al., 2002, MNRAS, 333, 133

Marinoni C., Hudson M.J., 2002, ApJ, 569, 101

Martínez H.J., Zandivarez A., Merchán M.E., Domínguez M.J.L., 2002, preprint (astro-ph/0208425)

Mathis H., Lemson G., Springel V., Kauffmann G., White S.D.M., Eldar A., Dekel A., 2002, MNRAS, 333, 739

McClelland J., Silk, J., 1977, ApJ, 217, 331

Mo H.J., White S.D.M., 1996, MNRAS, 282, 347

Mo H.J., White S.D.M., 2002, MNRAS, 336, 112

Moore B., Governato F., Quinn T., Stadel J., Lake G., 1998, ApJ, 499, L5

Muriel H., Valotto C.A., Lambas D.G., 1998, ApJ, 506, 540

Navarro J.F., Frenk C.S., White S.D.M., 1997, ApJ, 490, 493

Neyman J., Scott E.L., 1952, ApJ, 116, 144

Norberg P., et al., 2002, MNRAS, 332, 827

Peacock J.A., Smith R.E., 2000, MNRAS, 318, 1144

Pearce F.R., Thomas P.A., Couchman H.M.P., Edge A.C., 2000, MNRAS, 317, 1029

Power C., Navarro J.F., Jenkins A., Frenk C.S., White S.D.M., Springel V., Stadel J., Quinn T., 2002, preprint (astro-ph/0201544)

Press W.H., Teukolsky S.A., Vetterling W.T., Flannery B.P., 1992, Numerical Recipes (Cambridge: Cambridge University Press)

Pryke C., Halverson N.W., Leitch E.M., Kovac J., Carlstrom J.E., Holzapfel W.L., Dragovan M., 2002, ApJ, 568, 46

Ramella M., Pisani A., Geller M.J., 1997, AJ, 113, 483

Ramella M., et al., 1999, A&A, 342, 1

Schechter P., 1976, ApJ, 203, 297

Shectman S.A., Landy S.D., Oemler A., Tucker D.L., Lin H., Kirshner R.P., Schechter P.L., 1996, ApJ, 470, 172

Scoccimarro R., Sheth R.K., Hui L., Jain B., 2001, ApJ, 546, 20

Scranton R., 2002a, MNRAS, 332, 697

Scranton R., 2002b, preprint (astro-ph/0205517)

Seljak U., 2000, MNRAS, 318, 203

Sheth R.K., Tormen, G., 1999, MNRAS, 308, 119

Sheth R.K., Diaferio A., 2001, MNRAS, 322, 901

Sheth R.K., Mo H.J., Tormen G., 2001, MNRAS, 323, 1

Smith R.E., et al., 2002, preprint (astro-ph/0207664)

Somerville R.S., Primack J.R., 1999, MNRAS, 310, 1087

Tegmark M., Hamilton A.J.S., Xu Y., 2002, MNRAS, 335, 887

Trentham N., Hodgkin S., 2002, MNRAS, 333, 423

van den Bosch F.C., 2002, MNRAS, 332, 456

van Dokkum P.G., Franz M., Kelson D.D., Illingworth G.D., Fisher D., Fabricant D., 1998, ApJ, 500, 714

Verde L., Oh S.P., Jimenez R., 2002, MNRAS, 336, 541

White M., 2001, MNRAS, 321, 1

White M., 2002, preprint (astro-ph/0207185)

White S.D.M., Rees M.J., 1978, MNRAS, 183, 341

White S.D.M., Frenk C.S., 1991, ApJ, 379, 52

Willmer C.N.A., Da Costa L.N., Pellegrini P.S., 1998, AJ, 115, 869

Yang X., Mo H.J., van den Bosch F.C., 2002, preprint (astro-ph/0207019), paper 1

York D., et al., 2000, AJ, 120, 1579

Zehavi I., et al., 2002, ApJ, 571, 172

## APPENDIX A: THE TWO-POINT CORRELATION FUNCTION

The two-point correlation function of the evolved, non-linear dark matter mass distribution is given by

$$\xi_{\text{dm}}(r) = \int_0^\infty \frac{dk}{k} \Delta_{\text{NL}}^2(k) \frac{\sin kr}{kr} \quad (\text{A1})$$

Here

$$\Delta_{\text{NL}}^2(k) = \frac{1}{2\pi^2} k^3 P_{\text{NL}}(k) \quad (\text{A2})$$

is the dimensionless form of the evolved, non-linear power-spectrum  $P_{\text{NL}}(k)$ . Throughout this paper we use the fitting function for  $\Delta_{\text{NL}}^2(k)$  given by Smith et al. (2002), and compute  $\xi_{\text{dm}}(r)$  using equation (A1).

For what follows, we split this correlation function in two parts:

$$\xi_{\text{dm}}(r) = \xi_{\text{dm}}^{1\text{h}}(r) + \xi_{\text{dm}}^{2\text{h}}(r). \quad (\text{A3})$$

Here  $\xi_{\text{dm}}^{1\text{h}}$  corresponds to pairs within the same halo (the “1-halo” term), while  $\xi_{\text{dm}}^{2\text{h}}$  describes the correlation between

dark matter particles that occupy different haloes (the “2-halo” term). The 1-halo term is given by

$$\xi_{\text{dm}}^{\text{1h}}(r) = \int_0^\infty dk k^2 \frac{\sin kr}{kr} \int_0^\infty dM n(M) [\hat{\delta}(M; k)]^2 \quad (\text{A4})$$

where

$$\hat{\delta}(M; k) = \int_0^{r_v} \frac{\rho(r)}{\bar{\rho}} e^{-ik \cdot r} d^3 r \quad (\text{A5})$$

is the Fourier transform of the halo density profile  $\rho(r)$ , truncated at the virial radius  $r_v$  (e.g., Neyman & Scott 1952; McClelland & Silk 1977; Seljak 2000; Ma & Fry 2000; Scoccimarro et al. 2001). We assume that  $\rho(r)$  has the NFW form

$$\rho(r) = \frac{\bar{\delta} \bar{\rho}}{(r/r_s)(1+r/r_s)^2}, \quad (\text{A6})$$

where  $r_s$  is a characteristic radius,  $\bar{\rho}$  is the average density of the Universe, and  $\bar{\delta}$  is a dimensionless amplitude which can be expressed in terms of the halo concentration parameter  $c = r_v/r_s$  as

$$\bar{\delta} = \frac{180}{3} \frac{c^3}{\ln(1+c) - c/(1+c)}. \quad (\text{A7})$$

(cf., Navarro, Frenk & White 1997). Numerical simulations show that  $c$  is correlated with halo mass, and we use the relation given by Eke, Navarro & Steinmetz (2001), converted to the  $c$  appropriate for our definition of halo mass. Substitution of (A6) in (A5) yields, after some algebra,

$$\hat{\delta}(M; k) = 4\pi \bar{\delta} r_s^3 \left[ \mathcal{C} + \mathcal{S} - \frac{\sin(kr_v)}{kr_s + kr_v} \right] \quad (\text{A8})$$

(Scoccimarro et al. 2001). Here

$$\mathcal{C} = \cos(kr_s) [\text{Ci}(kr_s + kr_v) - \text{Ci}(kr_s)] \quad (\text{A9})$$

$$\mathcal{S} = \sin(kr_s) [\text{Si}(kr_s + kr_v) - \text{Si}(kr_s)] \quad (\text{A10})$$

with  $\text{Ci}(x) = -\int_x^\infty dt \cos(t)/t$  and  $\text{Si}(x) = \int_0^x dt \sin(t)/t$  the cosine and sine integrals, respectively.

In order to compute the galaxy-galaxy two-point correlation function,  $\xi_{\text{gg}}(r)$  we use the same 1-halo and 2-halo split as before:

$$\xi_{\text{gg}}(r) = \xi_{\text{gg}}^{\text{1h}}(r) + \xi_{\text{gg}}^{\text{2h}}(r). \quad (\text{A11})$$

For the 1-halo term we need to specify the distribution of galaxies in individual haloes, while the 2-halo term is given by the correlation of the population of dark matter haloes.

Consider all galaxies with luminosities in the range  $[L_1, L_2]$ , and let  $\xi_{\text{gg}}(r)$  correspond to the two-point correlation function of this subset of galaxies. By definition, the total number of pairs of galaxies *per comoving volume* in this luminosity range that have separations in the range  $r \pm dr/2$  is

$$n_{\text{pair}} = \frac{\bar{n}_g^2}{2} [1 + \xi_{\text{gg}}(r)] 4\pi r^2 dr. \quad (\text{A12})$$

where the factor 1/2 corrects for double counting of each pair. Here  $\bar{n}_g$  is the mean number density of galaxies with  $L \in [L_1, L_2]$  which is given by

$$\bar{n}_g = \int_0^\infty n(M) \langle N(M) \rangle dM, \quad (\text{A13})$$

and  $\langle N(M) \rangle$ , given by equation (10), gives the mean number of galaxies in the specified luminosity range for haloes of mass  $M$ .

Consider a galaxy with  $L \in [L_1, L_2]$  that lives in a halo of mass  $M_1$ . There are, on average,  $n(M_2) 4\pi r^2 dr$  dark matter haloes with mass  $M_2$  that are separated from this galaxy by a distance in the range  $r \pm dr/2$ . In each of these haloes there are on average  $\langle N(M_2) \rangle$  galaxies that also have a luminosity in the range  $[L_1, L_2]$ . Integrating over the halo mass function, and taking account of the clustering properties of dark matter haloes, we obtain the *excess* number  $N_+$  of galaxy pairs *per galaxy in a halo of mass  $M_1$*  with separations in the range  $r \pm dr/2$ :

$$N_+(M_1) = 4\pi r^2 dr \times \int_0^\infty n(M_2) \langle N(M_2) \rangle \xi_{\text{hh}}(r; M_1, M_2) dM_2. \quad (\text{A14})$$

Here  $\xi_{\text{hh}}(r; M_1, M_2)$  is the cross correlation between dark matter haloes of mass  $M_1$  and  $M_2$ . Note that we implicitly assume that all galaxies in a given halo are located at the halo center. Since the separation between individual haloes is typically much larger than the separation between galaxies in the same halo, this simplification does not influence the results.

Multiplying  $N_+(M_1)$  with  $\langle N(M_1) \rangle$  and integrating over the halo mass function gives the total excess number of galaxy pairs *per comoving volume* with separations in the required range. Combining this with equation (A12) yields

$$\bar{n}_g^2 \xi_{\text{gg}}^{\text{2h}}(r) 4\pi r^2 dr = \int_0^\infty n(M_1) \langle N(M_1) \rangle N_+(M_1) dM_1. \quad (\text{A15})$$

What remains is to specify the dark halo correlation function  $\xi_{\text{hh}}(r; M_1, M_2)$ . Mo & White (1996) developed a model, based on the Press-Schechter formalism, that describes the bias of dark matter haloes of mass  $M$  with respect to the dark matter mass distribution. According to this,

$$\xi_{\text{hh}}(r; M_1, M_2) = b(M_1) b(M_2) \xi_{\text{dm}}^{\text{2h}}(r), \quad (\text{A16})$$

We use the functional form of  $b(M)$  suggested by Sheth, Mo & Tormen (2001), which takes account of ellipsoidal collapse, and which has been shown to accurately match the correlation function of dark matter haloes in *N*-body simulations (Jing 1998; Sheth & Tormen 1999):

$$b(M) = 1 + \frac{1}{\sqrt{a} \delta_c(z)} \left[ \sqrt{a} (a\nu^2) + \sqrt{a} b (a\nu^2)^{1-c} - \frac{(a\nu^2)^c}{(a\nu^2)^c + b(1-c)(1-c/2)} \right], \quad (\text{A17})$$

with  $a = 0.707$ ,  $b = 0.5$ ,  $c = 0.6$  and  $\nu = \delta_c/\sigma(M)$ . This bias is defined for haloes at  $z = 0$ . In Appendix B we describe how to compute the bias of haloes and galaxies at  $z > 0$ .

Substituting equations (A16) and (A14) in (A15) yields

$$\xi_{\text{gg}}^{\text{2h}}(r) = \bar{b}^2 \xi_{\text{dm}}^{\text{2h}}(r), \quad (\text{A18})$$

with

$$\bar{b} = \frac{1}{\bar{n}_g} \int_0^\infty n(M) \langle N(M) \rangle b(M) dM. \quad (\text{A19})$$

Equations (A18) and (A19) specify the 2-halo term of  $\xi_{\text{gg}}(r)$ . Using a similar analysis as above, one obtains the 1-halo term of the galaxy correlation function as

$$\frac{\bar{n}_g^2}{2} \xi_{gg}^{1h}(r) 4\pi r^2 dr = dr \int_0^\infty n(M) \langle N_{\text{pair}}(M) \rangle f(r) dM, \quad (\text{A20})$$

where  $\langle N_{\text{pair}}(M) \rangle$  is the mean number of *pairs* in haloes of mass  $M$ , and  $f(r)$  gives the corresponding distribution of pair separations (e.g., Berlind & Weinberg 2002). Neither  $\langle N_{\text{pair}}(M) \rangle$  nor  $f(r)$  can be obtained from the CLF. In order to compute  $\xi_{gg}^{1h}(r)$ , additional assumptions have therefore to be made (see Section 6). The 1-halo term, on the other hand, depends only on  $\langle N(M) \rangle$  and is therefore completely specified by the CLF.

## APPENDIX B: THE EFFECTIVE BIAS OF GALAXIES AT NON-ZERO REDSHIFT

Dark matter haloes at redshift  $z$  are biased with respect to the dark matter mass distribution at  $z$  according to

$$\xi_{hh}(r, z; M_1, M_2) = b(M_1, z) b(M_2, z) \xi_{dm}^{2h}(r, z) \quad (\text{B1})$$

For this same population of haloes one can define a second bias according to

$$\xi_{hh}(r, 0; M_1, M_2) = b_0(M_1, z) b_0(M_2, z) \xi_{dm}^{2h}(r, 0) \quad (\text{B2})$$

where  $b_0(M, z)$  describes the bias at  $z = 0$  of the *descendants* of haloes that have mass  $M$  at redshift  $z$  (Fry 1996; Mo & White 1996, 2002).  $b_0(M, z)$  can be expressed in terms of the bias  $b(M)$  at  $z = 0$  given by equation (A17) as

$$b_0(M, z) = 1 + \frac{D(0)}{D(z)} [b(M) - 1] \quad (\text{B3})$$

(which is accurate to leading order), with  $D(z)$  the linear growth rate at redshift  $z$ . On sufficiently large scales, which are still in the linear regime,

$$\xi_{hh}(r, z; M_1, M_2) = \left( \frac{D(z)}{D(0)} \right)^2 \xi_{hh}(r, 0; M_1, M_2) \quad (\text{B4})$$

so that

$$\xi_{hh}(r, z; M_1, M_2) = b_{\text{eff}}(M_1, z) b_{\text{eff}}(M_2, z) \xi_{dm}^{2h}(r, 0) \quad (\text{B5})$$

with

$$b_{\text{eff}}(M, z) = \frac{D(z)}{D(0)} + b(M) - 1 \quad (\text{B6})$$

Substituting  $b(M)$  in equation (A19) with  $b_{\text{eff}}(M, z)$  one obtains the effective bias of *galaxies* at redshift  $z$  with luminosities in the range  $L_1 < L < L_2$ :

$$\bar{b}_{\text{eff}}(z) \equiv \left( \frac{\xi_{gg}^{2h}(r, z)}{\xi_{dm}^{2h}(r, 0)} \right)^{1/2} = \frac{D(z)}{D(0)} + \bar{b} - 1 \quad (\text{B7})$$

with

$$\bar{b} = \left( \frac{\xi_{gg}^{2h}(r, 0)}{\xi_{dm}^{2h}(r, 0)} \right)^{1/2} \quad (\text{B8})$$

the average bias of galaxies with  $L_1 < L < L_2$  at  $z = 0$ , which can be obtained from the CLF using equations (9) and (10).